minerals

MDPI

Article

Mineral Chemistry of Pyrochlore Supergroup Minerals from the Boziguoer Nb-Ta-Zr-Rb-REE Deposit, NW China: Implications for Nb Enrichment by Alkaline Magma Differentiation

Zhenghao Sun [1,2,3], Kezhang Qin [1,2,3,*], Yajing Mao [3], Dongmei Tang [3], Fangyue Wang [4], Noreen J. Evans [5] and Qifeng Zhou [6]

1. Xinjiang Research Center for Mineral Resource, Xinjiang Institute of Ecology and Geography, Chinese Academy of Sciences, Urumqi 830011, China; sunzhenghao18@mails.ucas.ac.cn
2. College of Earth and Planetary Sciences, University of Chinese Academy of Sciences, Beijing 100049, China
3. Key Laboratory of Mineral Resources, Institute of Geology and Geophysics, Chinese Academy of Sciences, Beijing 100029, China; maoyajing@mail.iggcas.ac.cn (Y.M.); tdm@mail.iggcas.ac.cn (D.T.)
4. School of Resources and Environmental Engineering, Hefei University of Technology, Hefei 230009, China; fywang@hfut.edu.cn
5. School of Earth and Planetary Sciences/John de Laeter Centre, Curtin University, Perth 6845, Australia; noreen.evans@curtin.edu.au
6. Institute of Mineral Resources Research, China Metallurgical Geology Bureau, Beijing 101300, China; zhouqifeng85@163.com

* Correspondence: kzq@mail.iggcas.ac.cn

check for updates

Citation: Sun, Z.; Qin, K.; Mao, Y.; Tang, D.; Wang, F.; Evans, N.J.; Zhou, Q. Mineral Chemistry of Pyrochlore Supergroup Minerals from the Boziguoer Nb-Ta-Zr-Rb-REE Deposit, NW China: Implications for Nb Enrichment by Alkaline Magma Differentiation. *Minerals* **2022**, *12*, 785. https://doi.org/10.3390/min12070785

Academic Editors: Massimo D' Antonio and Ilenia Arienzo

Received: 6 May 2022
Accepted: 17 June 2022
Published: 21 June 2022

Abstract: Alkaline rocks are generally enriched in rare metals (e.g., Nb, Ta, and Zr) and rare earth elements (REE), but the key factors controlling Nb-Ta-REE enrichment remain unclear. The Boziguoer Nb (Ta-Zr-Rb-REE) deposit in Southwest Tianshan (northern margin of Tarim Basin) is China's largest, with reserves of 0.32 Mt Nb_2O_5 and 0.02 Mt Ta_2O_5. It is an alkaline felsic complex 4.45 km in length and 0.5–1.3 km in width, composed of alkalic granite and syenite, which can be subdivided into syenite I and syenite II. The main minerals in each lithofacies are the same (albite, K-feldspar, quartz, arfvedsonite and aegirine). The Nb in the deposit is mainly hosted in pyrochlore supergroup minerals, ubiquitous in alkalic granite and syenite of the Boziguoer deposit. The wide variation in cations (Ca, Na, REE, U, Th) in the A-site further classifies the Boziguoer pyrochlore supergroup minerals as fluornatropyrochlore, fluorcalciopyrochlore and fluorkenopyrochlore. All Boziguoer pyrochlore supergroup minerals are Nb-rich and Ta-poor at the B-site and dominated by F at the Y-site. These cation occurrence illustrate a new mechanism of substitution in the Boziguoer pyrochlore supergroup minerals ($2Ca^{2+} + Ti^{4+} + 4Ta^{5+} = REE^{3+} + A\text{-}V + 5Nb^{5+}$, where A-V is the A-site vacancy). This substitution mechanism is different from that in the pyrochlore supergroup minerals from other rocks such as carbonatite and nepheline syenite, which are dominated by the replacement of Ba (Rb, Sr) with Ca+ Na + A-V. In addition, the substitution of REE (mainly La, Ce) for Ca in the Boziguoer pyrochlore supergroup minerals is likely a result of either REE enrichment or a change in the REE partition coefficient during the evolution of the alkaline magma. Both the pyrochlore supergroup minerals and their host rocks display negative large ion lithophile element (LILE; K, Rb, Sr, and Ba) anomalies, positive high-field-strength element (HFSE) anomalies and light rare earth element (LREE) enrichment with negative Eu anomalies. This is consistent with the crystallization of the pyrochlore supergroup minerals from the magma rather than from hydrothermal fluids, suggesting a magmatic origin. These findings indicate that the mechanisms of pyrochlore supergroup minerals crystallization in alkaline magma may be significantly different from those in carbonatite and nepheline syenite, and that magmatic differentiation processes may have played a role in the enrichment of the Boziguoer deposit by Nb.

Keywords: Boziguoer Nb-Ta-Zr-REE deposit; niobium mineralization; mineral chemistry of pyrochlore; new element substitution mechanism; alkaline felsic rocks; northern margin of Tarim basin

1. Introduction

Niobium is a critical metal with many important uses [1,2], and while there are numerous studies focused on carbonatite- and granitic pegmatite-related Nb deposits [3–7], Nb deposits associated with alkaline rocks show the opposite trend. Thus, the key factors controlling niobium mineralization in alkaline rocks are relatively poorly understood. Alkaline rocks are commonly enriched in rare metals, high-field-strength elements (HFSE; Nb and Ta), rare earth elements (REE) and radioactive elements [8–12]. The main issue regarding Nb enrichment in these rocks is whether the minerals hosting the rare metal were crystallized at the magmatic stage or formed during post-magmatic alteration processes, when hydrothermal fluids remobilized and enriched the rare metal element cargo of the primary magma [13–16]. The Boziguoer Nb-Ta-Zr-Rb-REE deposit in Southwest Tianshan, NW China, was discovered in 1998 and is currently China's largest Nb deposit. It is also a 'type' example of Nb enrichment associated with alkaline magma. Boziguoer contains reserves of 0.32 Mt Nb_2O_5, 0.02 Mt Ta_2O_5 and 0.7 Mt $ZrSiO_4$, and associated REE reserves of 0.2 Mt with 0.64 Mt Rb_2O [17]. Moreover, it is associated with a 1100-km-long belt of alkaline rocks in SW Tianshan and is contemporaneous with Permian Tarim Plume activity (~280 Ma). These features mean that the studying of the Boziguoer deposit has both economic and scientific significance. According to field observations, some studies have proposed that Boziguoer Nb mineralization was associated with magmatic differentiation processes [18,19], whereas others suggest that later hydrothermal activity played an important role [20]. Resolving this genetic paradigm will have implications not only for Nb mineralization in the Boziguoer deposit, but also for our understanding of the whole of the NW Tarim alkalic intrusion belt.

Pyrochlore supergroup minerals are common ore phases in Nb deposits [21–25] and are the most important minerals hosting Nb in the Boziguoer deposit [17,26–29]. Previous work discovered a new pyrochlore supergroup mineral (fluornatropyrochlore) in the Boziguoer deposit [20]. The chemistry of pyrochlore group minerals can be used to elucidate the crystallization environment, equilibrium melt properties and magma evolution [23,30–41].

This study uses major and trace element analyses of pyrochlore supergroup minerals from different lithofacies of mineralized rock from the Boziguoer deposit in an effort to resolve the genesis of Nb mineralization. The compositional results are further compared with those from carbonatite and nepheline syenite in order to investigate the evolution of pyrochlore supergroup minerals' composition during magma differentiation.

2. Regional Geology

The Boziguoer alkaline felsic rock-related Nb-Ta-Zr-Rb-REE deposit is located in the Southern Tianshan orogenic belt (Figure 1b), which is an important part of the Central Asia orogenic belt (CAOB, Figure 1a). The CAOB is a giant suture zone formed by the formation, evolution and extinction of the Ancient Asian Ocean among the Siberian craton, Sino-Korea plate and Tarim plate. It is a typical accretionary orogenic belt, characterized by the development of a large number of magmatic complexes [42,43]. The superposition of Permian mantle plumes in the Tarim basin resulted in complex metallogenesis [44–48], and Carboniferous–Permian magmatic rocks with associated porphyry-epithermal Cu-Au and Cu-Ni sulfide mineralization, particularly well developed [43,49–58]. The Southern Tianshan region of China consists of the Central Tianshan block, Southern Tianshan orogenic belt and the northern margin of the Tarim block, from north to south. The Central Tianshan block is an ancient continental microplate, whose basement rocks are primarily composed of middle Neoproterozoic gneiss, schist and marble. The basement rocks are directly covered by Sinian carbonates and moraines. In the south, the Central Tianshan block and Southern Tianshan orogenic belt are bounded by the Yili-Centre Tianshan Suture Fracture zone (YCSF). The Southern Tianshan orogenic belt is located between the Yili–Kazakhstan and Tarim–Karakum plates, and extends to the border of Xinjiang and Gansu in China, through Uzbekistan, Tajikistan, Kyrgyzstan and Kazakhstan. It is a collisional orogenic belt formed during the subduction and closure of the Southern Tianshan ocean basin in the late Precambrian. It then evolved gradually, accreting the continental blocks on either side and the complexes between them [59]. The composition of the Southern Tianshan orogenic belt is very complex, including not only the Precambrian basement rocks and oceanic accretion material, but also continental margin/shallow marine sediments from the northern margin of the Tarim block. The northern margin of the Tarim block is separated by the Tarim northern fault. The interior of the Tarim block is covered by desert, and most of the bedrock at the northern margin was covered by unconsolidated or semi-consolidated sedimentary rocks or sediments in the Meso-Cenozoic, with sparse outcrops in the middle and easternmost parts.

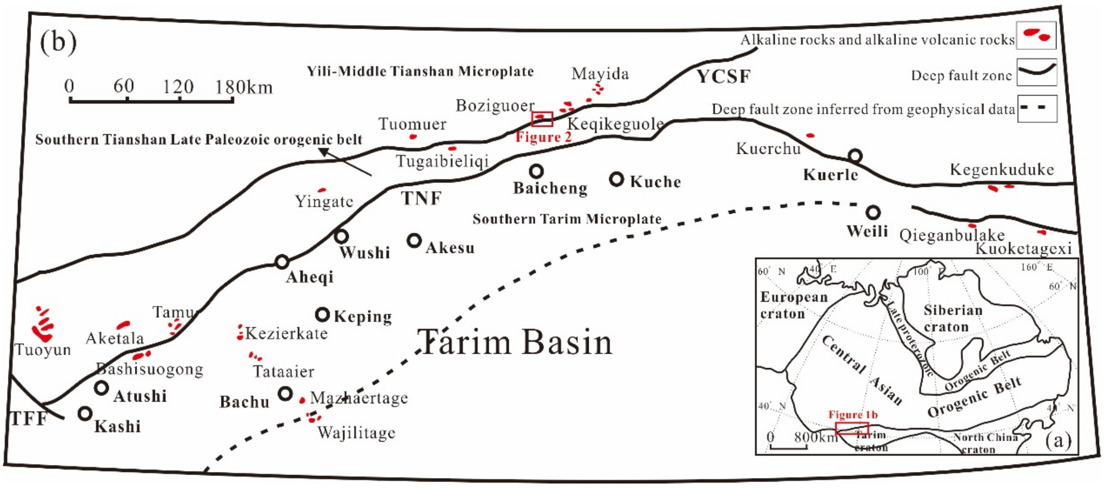

Figure 1. (**a**) Tectonic units and location of Southern Tianshan region in Xinjiang, NW China (modified from [58]); (**b**) distribution of the Boziguoer deposit in the Southern Tianshan region and coeval alkaline felsic rocks in the Tarim north rim (modified from [60,61]).

The northern margin of the Tarim basin and adjacent areas were intruded by a series of alkaline rocks in the late Carboniferous–Permian period (Figure 1b), including alkaline granite, quartz syenite, syenite, aegirine syenite and aegirine nepheline syenite. These extend from Atushi in the west, to the east of Yuli, and are distributed in a belt approximately 1100 km long [60,61]. Regional geological work is relatively weak, and the mineral resources discovered are very limited, including some rare metal and REE deposits. The host rock types are mainly alkaline granite, syenite, carbonate and alkaline pegmatite (accompanied by gem and jade mineralization) [62].

The Boziguoer deposit is the largest in this alkaline rock belt and considered the most representative of the type. It is located 43 km north of Baicheng county, east of the alkaline rock belt, on the southern slope of Hariketao Mountain in the western section of the Tianshan Mountain Range. Intrusive rocks are not well developed in this region, with only the Boziguoer alkaline felsic rock developed in the central parts. Volcanic rocks are relatively well represented, and volcanic activity can be divided into three cycles: Silurian, Early Carboniferous and Early Permian.

3. Geology of the Boziguoer Large-Scale Deposit

The exposed strata in the Boziguoer mining area comprise the Silurian Qiongkusitai Formation (S_3g), with gray marble, argillaceous siltstone, biotite quartz schist and crystalline limestone. Fold structures are not well developed, and the stratum can generally be described as having a monoclinal structure with an east–west strike and a northward dip. The Boziguoer complex is an east–west fish-shaped stock that intrudes into the upper Silurian marble (Figure 2). It is around 4.45 km long and 0.5–1.3 km wide, covering an area of approximately 2.6 km^2. The complex is composed of biotite alkali feldspar granite (east) and alkaline felsic rock containing aegirine and arfvedsonite (west). The alkaline felsic rock is the main ore-bearing rock and is composed of multiple lithofacies. Our pyrochlore supergroup mineral-bearing samples were all collected from the alkaline felsic rock. The boundary between ore-bearing rock and biotite alkaline granite is the NNE-trending fault (F2), with an NWW-trending fault (F3) and Silurian Qiongkushitai Formation marble to the south (Figure 2).

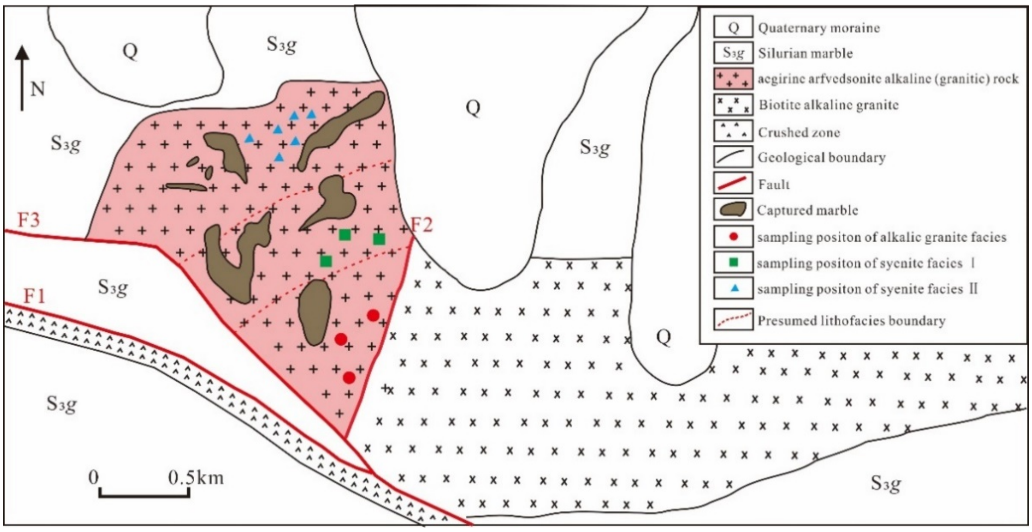

Figure 2. Simplified geologic map of the Boziguoer intrusion and sample locations (modified after [28,29]).

The ore-bearing rock is an elliptic stock distributed in the central and western part of the ore district. It is approximately 1.2 km long, 1 km wide and around 1.2 km^2 in area. The strike is NWW, and the dip direction is NNE at an angle of around 70°. The whole western intrusion was mineralized with Nb, accompanied by Ta, Rb, Zr and REE [14]. The ore-bearing alkaline felsic rock can be divided into three types: aegirine arfvedsonite alkaline feldspar granite (alkalic granite facies), aegirine arfvedsonite quartz alkaline feldspar syenite (syenite facies I) and aegirine arfvedsonite alkaline feldspar syenite (syenite facies II) [17]. A detailed description of each is given below. There were no obvious lithologic boundaries and cross-cutting relationships between lithofacies noted in the field, so a gradual transition is inferred. The relative positions of different lithofacies can be seen from the sampling positions (Figure 2). Previous zircon U-Pb geochronology on ore-bearing rock showed that the mineralized rock was formed in the Early Permian (280.9–291.6 Ma [27]; 290.1 ± 1.4 Ma [63]). Alteration is relatively weak, mainly including chloritization, epidotization, fluoridation and limonitization. According to preliminary evaluation, the Boziguoer deposit has reserves of 0.32 Mt Nb_2O_5 at 0.0418 wt.%, 0.02 Mt Ta_2O_5 at 0.0028 wt.%, 0.64 Mt Rb_2O at 0.0831 wt.%, 0.7 Mt $ZrSiO_4$ and 0.2 Mt ΣREE at 0.0765 wt.%. While Nb mineralization dominates, Boziguoer is considered to be a super-large Nb-Ta-Zr-Rb-REE deposit [17,61].

Detailed petrographic features of the mineralized rock lithofacies are given in an earlier study [17] and summarized below. The alkalic granite facies (Figure 3a,b) has the highest content of quartz (20%–25%) and the least arfvedsonite (5%–10%) and aegirine (3%–5%). This massive, gray–white, medium–fine-grained rock also contains albite (35%–45%) and K-feldspar (20%–25%) [17]. Syenite facies I (Figure 3c,d) contains albite (45%–55%), K-feldspar (20%–30%), arfvedsonite (8%–15%), aegirine (5%–8%) and quartz (5%–8%). It has the same crystal size and massive structure as the alkalic granite facies but is slightly darker in color. Syenite facies II (Figure 3e,f) has the highest content of arfvedsonite (10%–15%) and aegirine (5%–8%) and the lowest content of quartz (0%–3%). It is the only rock with banding, formed by the alignment of dark alkaline minerals, with gray–white to light blue color.

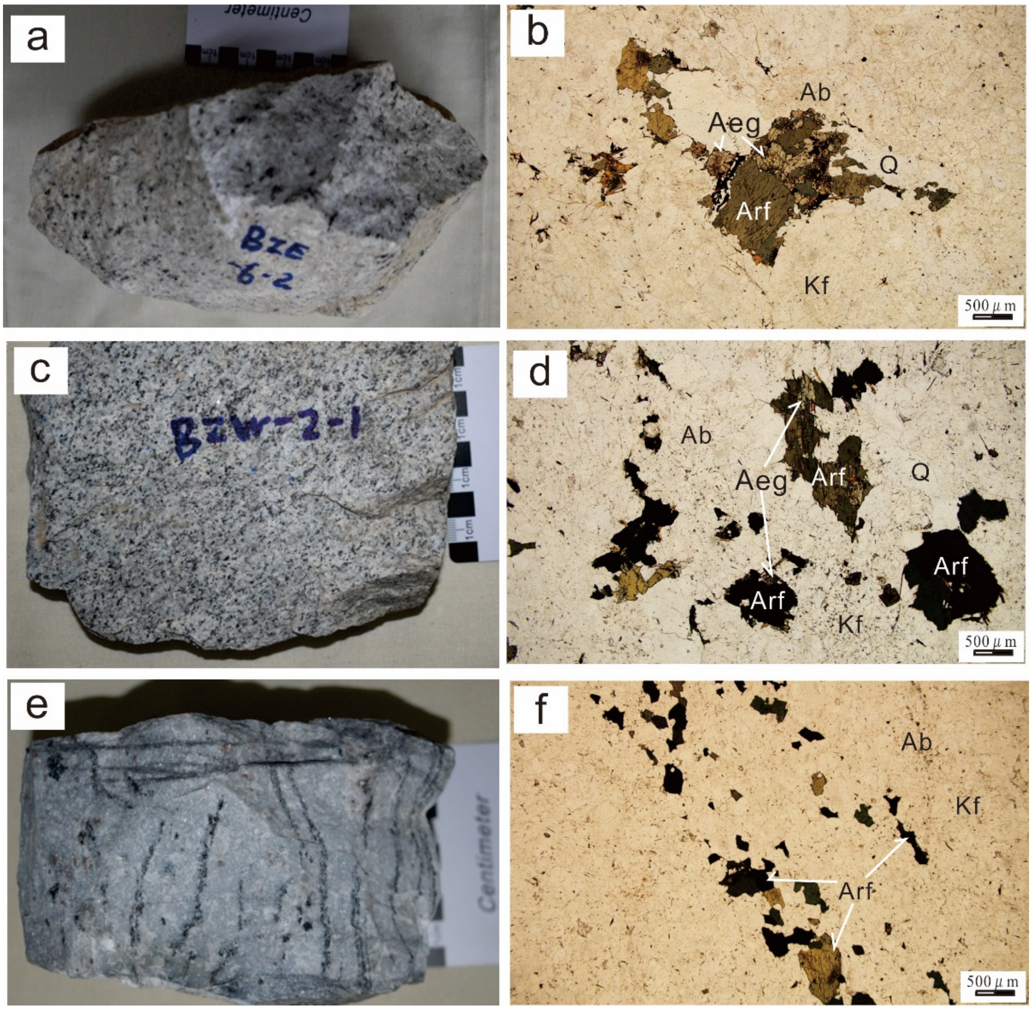

Figure 3. Hand sample images and microphotographs of main rocks of the Boziguoer intrusion. (**a**,**b**) = Alkalic granite facies; (**c**,**d**) = syenite facies I; (**e**,**f**) = syenite facies II. Abbreviations: Q = quartz, Ab = albite, Kf = K-feldspar, Aeg = aegirine, Arf = arfvedsonite.

The main minerals of each lithofacies are the same (albite, K-feldspar, quartz, arfvedsonite and aegirine; Figure 4a), but the relative abundance of minerals, crystal size and structure distinguish the lithofacies from one another. Quartz is mostly euhedral and subhedral. Albite occurs as euhedral, columnar and platy crystals with a composition of An <5.0 (unpublished data). K-feldspar is euhedral and columnar. Greenish blue, highly pleochroic arfvedsonite grains are allographic–subhedral columnar, and some are interstitial and enclose feldspar and quartz crystals. These grains have amphibole cleavage (56°). Green to black green aegirine is highly pleochroic, allographic–subhedral (0.1–0.5 mm) and always occurs with arfvedsonite. It also has pyroxene cleavage (87°). Semi-euhedral and euhedral 0.1–2.5 mm arfvedsonite grains are interstitial between alkali feldspar and quartz. The arfvedsonite and aegirine are intergrown, and their aggregates can form bands. The interstitial texture and inclusion of feldspar and quartz indicate that arfvedsonite and aegirine crystallized later than these minerals (Figure 4b,c).

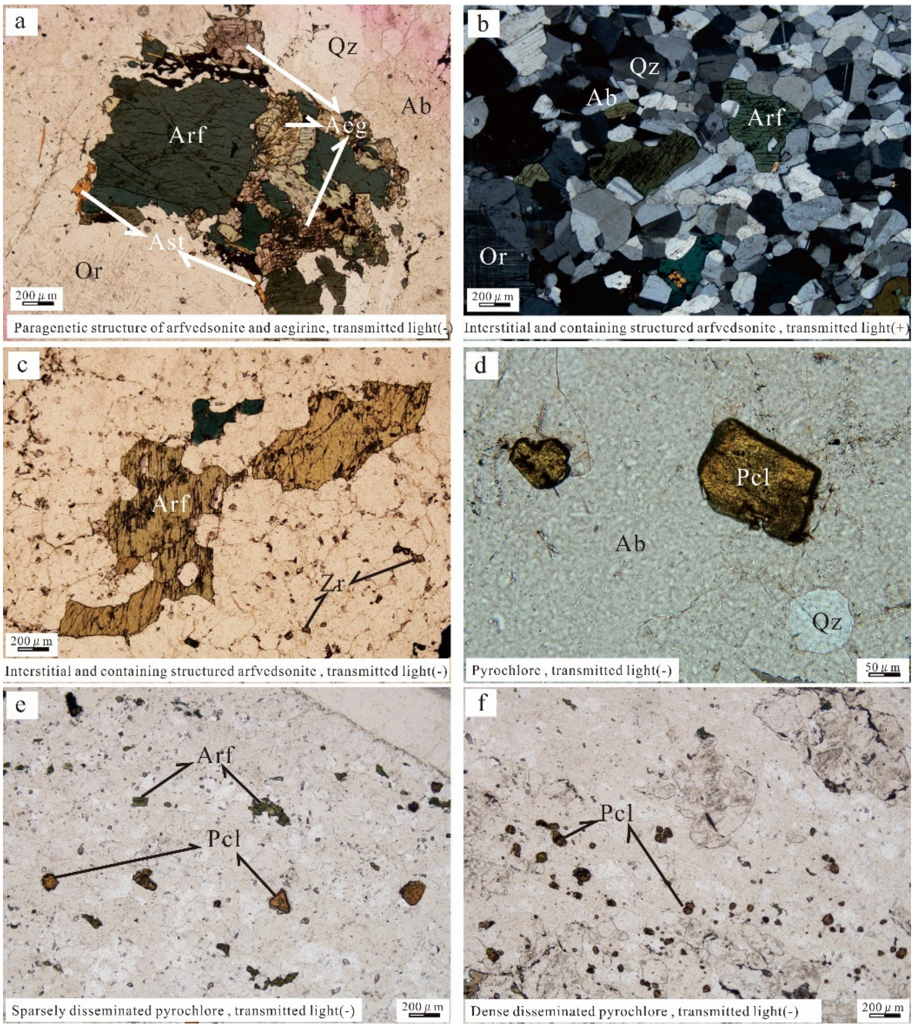

Figure 4. Microphotographs showing the textures of Boziguoer alkaline granite ((**a**,**d**) = alkalic granite facies, (**b**,**e**) = syenite facies I, (**c**,**f**) = syenite facies II). Arf = arfvedsonite, Aeg = aegirine, Ast = astrophyllite, Qz = quartz, Or = orthoclase, Ab = albite, Pcl = pyrochlore supergroup minerals.

Accessory minerals mainly comprise the pyrochlore supergroup minerals, zircon, astrophyllite, thorite, monazite, bastnasite, xenotime and fluorite. Most form either granular aggregates, single crystals between gangue mineral grains or are encased in early alkaline feldspar. The distribution of all accessory phases is disseminated, indicating late formation of the ore minerals. Combining our data (Table 1 and Supplementary Materials Table S1) with previous research results [28] shows that Nb and Ta are mainly hosted in the pyrochlore supergroup mineral, a small part of Nb occurs in astrophyllite, Rb and Cs are mainly hosted in astrophyllite, Zr is primarily found in zircon and REE are concentrated in monazite, xenotime and bastnaesite.

Table 1. Chemical composition of pyrochlore group minerals from the Boziguoer Nb deposit.

Number	BZ-Pcl-1-1	BZ-Pcl-1-2	BZ-Pcl-1-3	BZ-Pcl-1-4	BZ-Pcl-1-5	BZ-Pcl-1-6	BZ-Pcl-1-7	BZ-Pcl-1-8	BZ-Pcl-1-9	BZ-Pcl-1-10	BZ-Pcl-1-11
Rock	Alkalic granite facies										
F	2.40	2.46	2.20	2.17	2.17	2.42	2.40	2.30	2.28	1.88	2.06
Na_2O	7.26	6.80	6.24	6.86	6.91	7.50	6.91	6.38	6.44	4.48	5.97
Ta_2O_5	3.27	3.69	3.82	3.81	3.68	3.94	3.90	2.07	3.53	3.10	3.05
SiO_2	0	0	0	0	0.06	0	0	0	0	1.19	0
Nb_2O_5	60.2	59.1	58.8	58.3	59.0	58.5	58.2	58.6	56.8	54.6	55.3
ThO_2	0.13	0.23	0.22	0.13	0.28	0.25	0.27	0.82	0.85	0.43	0.69
UO_2	4.65	4.66	5.61	5.77	5.35	4.51	4.35	4.44	5.81	9.08	8.45
CaO	10.9	11.1	10.9	11.0	11.1	10.9	11.0	13.3	13.3	11.2	14.0
TiO_2	4.92	5.23	5.23	5.07	5.15	5.05	5.81	6.77	7.00	7.16	7.83
La_2O_3	1.43	1.30	1.45	1.32	1.23	0.98	1.17	0.38	0.40	0.35	0.53
Ce_2O_3	3.37	3.47	3.41	3.20	3.30	3.75	3.44	1.88	1.86	1.11	1.70
Fe_2O_3	0	0	0.01	0.11	0	0	0	0	0	0.29	0
Total	98.52	97.97	97.84	97.78	98.26	97.78	97.51	96.99	98.28	94.82	99.61
Structural formula (∑B-site cations = 2)/apfu											
Na	0.89	0.83	0.77	0.85	0.85	0.93	0.84	0.77	0.78	0.54	0.73
Ca	0.73	0.75	0.74	0.76	0.75	0.74	0.75	0.89	0.89	0.74	0.95
La	0.03	0.03	0.03	0.03	0.03	0.02	0.03	0.01	0.01	0.01	0.01
Ce	0.08	0.08	0.08	0.07	0.08	0.09	0.08	0.04	0.04	0.03	0.04
Th	0	0	0	0	0	0	0	0.01	0.01	0.01	0.01
U	0.07	0.07	0.08	0.08	0.08	0.06	0.06	0.06	0.08	0.13	0.12
∑A	1.8	1.76	1.7	1.8	1.79	1.85	1.76	1.78	1.82	1.45	1.86
Nb	1.71	1.69	1.68	1.68	1.69	1.69	1.66	1.65	1.61	1.53	1.58
Ta	0.06	0.06	0.07	0.07	0.06	0.07	0.07	0.03	0.06	0.05	0.05
Ti	0.23	0.25	0.25	0.24	0.24	0.24	0.28	0.32	0.33	0.33	0.37
Si	0	0	0	0	0	0	0	0	0	0.07	0
Fe	0	0	0	0.01	0	0	0	0	0	0.01	0
∑B	2	2	2	2	2	2	2	2	2	2	2
F=O	0.48	0.49	0.44	0.44	0.43	0.49	0.48	0.45	0.45	0.37	0.41
A-V	0.2	0.24	0.3	0.2	0.21	0.15	0.24	0.22	0.18	0.55	0.14

Table 1. *Cont.*

Number	BZ-Pcl-1-13	BZ-Pcl-1-14	BZ-Pcl-1-15	BZ-Pcl-1-16	BZ-Pcl-1-17	BZ-Pcl-1-18	BZ-Pcl-1-19	BZ-Pcl-1-20	BZ-Pcl-1-21	BZ-Pcl-1-22
Rock	Alkalic granite facies									
F	1.89	1.76	2.01	2.08	1.78	2.07	1.87	1.21	0.77	1.01
Na_2O	6.32	4.87	4.45	5.73	5.84	6.01	6.03	6.03	5.86	5.88
Ta_2O_5	2.7	2.29	3.07	2.81	2.79	1.73	2.28	2.2	4.07	4.21
SiO_2	0	0	0	0.04	1.49	0.34	0.22	0.09	0.14	0.18
Nb_2O_5	55.6	57.8	56.8	56.1	53.8	57.2	57.4	57.7	57.2	56.8
ThO_2	0.54	0.39	0.52	0.61	0.89	0.94	0.69	0.71	0.77	0.78
UO_2	8.33	8.42	8.46	8.21	8.14	4.24	4.31	4.31	4.27	4.42
CaO	14.2	14.1	14.4	13.5	13.1	15.8	16.3	16.3	15.8	15.6
TiO_2	8.05	7.45	7.85	7.23	7.33	7.03	6.94	7.04	7.02	7
La_2O_3	0.32	0.1	0.19	0.41	0.52	0.65	0.59	0.54	0.58	0.72
Ce_2O_3	1.39	0.8	1.12	1.52	1.81	2.18	2.02	1.95	2.06	2.31
Fe_2O_3	0.01	0.21	0.05	0	0	0	0.01	0.02	0	0
Total	99.34	98.22	98.85	98.24	97.45	98.27	98.64	98.07	98.53	98.89
Structural formula (∑B-site cations = 2)/apfu										
Na	0.77	0.58	0.53	0.7	0.71	0.73	0.73	0.73	0.7	0.71
Ca	0.95	0.93	0.95	0.92	0.88	1.06	1.09	1.09	1.05	1.04
La	0.01	0	0	0.01	0.01	0.02	0.01	0.01	0.01	0.02
Ce	0.03	0.02	0.03	0.04	0.04	0.05	0.05	0.04	0.05	0.05
Th	0.01	0.01	0.01	0.01	0.01	0.01	0.01	0.01	0.01	0.01
U	0.12	0.12	0.12	0.12	0.11	0.06	0.06	0.06	0.06	0.06
∑A	1.88	1.66	1.64	1.79	1.76	1.93	1.95	1.95	1.88	1.89
Nb	1.57	1.61	1.58	1.61	1.52	1.62	1.62	1.63	1.6	1.59
Ta	0.05	0.04	0.05	0.05	0.05	0.03	0.04	0.04	0.07	0.07
Ti	0.38	0.34	0.36	0.34	0.34	0.33	0.33	0.33	0.33	0.33
Si	0	0	0	0	0.09	0.02	0.01	0.01	0.01	0.01
Fe	0	0.01	0	0	0	0	0	0	0	0
∑B	2	2	2	2	2	2	2	2	2	2
F=O	0.37	0.34	0.39	0.42	0.35	0.41	0.37	0.24	0.15	0.2
A-V	0.12	0.34	0.36	0.21	0.24	0.07	0.05	0.05	0.12	0.11

Table 1. *Cont.*

Number	BZ-Pcl-1-23	BZ-Pcl-1-24	BZ-Pcl-1-25	BZ-Pcl-1-26	BZ-Pcl-1-27	BZ-Pcl-1-28	BZ-Pcl-1-29	BZ-Pcl-1-30	BZ-Pcl-1-31	BZ-Pcl-1-32	BZ-Pcl-1-33
Rock	Alkalic granite facies										
F	2.01	2.25	1.71	1.72	1.88	2.01	1.61	0.73	0.71	1.05	1.76
Na_2O	6.42	6.39	5.59	5.58	5.06	5.37	5.74	5.81	5.81	5.63	5.79
Ta_2O_5	2.41	2.3	3.08	3.22	3.41	2.97	3.33	3.05	3.22	2.11	2.51
SiO_2	0.22	0.66	2.85	1.71	1.87	0.39	0.18	0.11	0.09	0.2	0.1
Nb_2O_5	58.6	57.8	53.7	53.7	52.6	54.5	54.5	56.3	55.1	55.1	55.4
ThO_2	0.17	0.29	0.59	0.68	0.94	0.73	0.86	0.84	0.81	0.7	0.79
UO_2	6.73	6.06	8.15	8.97	8.51	9.36	8.79	8.59	8.64	8.8	8.39
CaO	11.3	11.4	14.6	15.1	14.1	14.5	14.3	15.4	14.4	14.4	14.4
TiO_2	5.07	5.16	7.53	7.49	7.2	7.75	7.53	7.41	7.55	7.64	7.53
La_2O_3	1.57	1.6	0.44	0.4	0.55	0.37	0.66	0.47	0.69	0.66	0.67
Ce_2O_3	3.36	3.47	1.32	1.22	1.74	1.26	1.93	1.15	1.98	1.99	1.95
Fe_2O_3	0.01	0	0	0.02	0.03	0	0.01	0.02	0	0.02	0
Total	97.83	97.41	99.51	99.77	97.90	99.13	99.48	99.83	98.92	98.22	99.32
Structural formula (∑B-site cations = 2)/apfu											
Na	0.8	0.79	0.65	0.67	0.61	0.66	0.71	0.71	0.71	0.7	0.71
Ca	0.78	0.78	0.93	1	0.94	0.98	0.98	1.03	0.98	0.98	0.98
La	0.04	0.04	0.01	0.01	0.01	0.01	0.02	0.01	0.02	0.02	0.02
Ce	0.08	0.08	0.03	0.03	0.04	0.03	0.05	0.03	0.05	0.05	0.05
Th	0	0	0.01	0.01	0.01	0.01	0.01	0.01	0.01	0.01	0.01
U	0.1	0.09	0.11	0.12	0.12	0.13	0.12	0.12	0.12	0.12	0.12
∑A	1.79	1.78	1.73	1.83	1.74	1.82	1.89	1.91	1.89	1.87	1.89
Nb	1.7	1.67	1.44	1.49	1.49	1.56	1.57	1.59	1.58	1.58	1.59
Ta	0.04	0.04	0.05	0.05	0.06	0.05	0.06	0.05	0.06	0.04	0.04
Ti	0.24	0.25	0.34	0.35	0.34	0.37	0.36	0.35	0.36	0.37	0.36
Si	0.01	0.04	0.17	0.11	0.12	0.02	0.01	0.01	0.01	0.01	0.01
Fe	0	0	0	0	0	0	0	0	0	0	0
∑B	2	2	2	2	2	2	2	2	2	2	2
F=O	0.41	0.45	0.32	0.34	0.37	0.4	0.32	0.14	0.14	0.21	0.35
A-V	0.21	0.22	0.27	0.17	0.26	0.18	0.11	0.09	0.11	0.13	0.11

Table 1. *Cont.*

Number	BZ-Pcl-2-1	BZ-Pcl-2-2	BZ-Pcl-2-3	BZ-Pcl-2-4	BZ-Pcl-2-5	BZ-Pcl-2-6	BZ-Pcl-2-7	BZ-Pcl-2-8	BZ-Pcl-2-9	BZ-Pcl-2-10
Rock	Syenite facies I									
F	3.11	3.08	3.1	3.61	3.15	3.19	3.13	3.22	3.36	3.21
Na_2O	5.12	4.69	3.46	2.15	5.28	5.43	5.32	5.31	5.48	5.65
Ta_2O_5	0.25	0.49	0.71	0.78	0.74	0.31	0.44	0.83	1.72	1.27
SiO_2	1.21	1.05	1.09	2.11	0.88	1.35	2.95	1.33	0.51	0.78
Nb_2O_5	64.1	64.1	64.3	64.2	63.5	65.1	63.2	64.5	63	62.1
ThO_2	0.21	1.29	0.82	1.08	0.88	0.32	0.62	0.81	0.45	1.21
UO_2	8.69	7.66	10.1	10	8.41	7.83	8.31	6.34	7.29	7.35
CaO	9.42	9.11	8.81	8.28	8.89	9.05	8.96	9.36	8.15	8.1
TiO_2	4.41	4.49	4.54	4.78	4.19	4.36	4.2	4.19	4.3	4.13
La_2O_3	0.39	0.53	0.26	0.29	0.18	0.69	0.53	0.31	0.71	1.11
Ce_2O_3	1.11	1.26	1.1	0.88	1.1	1.45	1.17	1.42	2.71	3.65
Fe_2O_3	0.42	0.38	0.23	0.39	0.02	0.06	0.06	0.04	0.31	0.35
Total	98.46	98.15	98.48	98.56	97.18	99.13	98.90	97.62	97.98	98.89
Structural formula (∑B-site cations = 2)/apfu										
Na	0.59	0.54	0.4	0.24	0.62	0.62	0.59	0.61	0.65	0.67
Ca	0.6	0.58	0.56	0.5	0.58	0.57	0.55	0.59	0.53	0.53
La	0	0.01	0.01	0	0	0.01	0.01	0	0.02	0.03
Ce	0.02	0.03	0.02	0.02	0.02	0.03	0.02	0.03	0.06	0.08
Th	0	0.02	0.01	0.01	0.01	0	0.01	0.01	0	0.02
U	0.11	0.1	0.13	0.13	0.11	0.1	0.11	0.08	0.1	0.1
∑A	1.33	1.27	1.13	0.9	1.36	1.34	1.3	1.33	1.35	1.43
Nb	1.71	1.71	1.71	1.65	1.74	1.73	1.65	1.72	1.73	1.72
Ta	0	0.01	0.01	0.01	0.01	0	0	0.01	0.03	0.02
Ti	0.2	0.2	0.2	0.2	0.19	0.19	0.18	0.19	0.2	0.19
Si	0.07	0.06	0.06	0.12	0.05	0.08	0.17	0.08	0.03	0.05
Fe	0.02	0.02	0.01	0.02	0	0	0	0	0.01	0.02
∑B	2	2	2	2	2	2	2	2	2	2
F=O	0.58	0.58	0.58	0.65	0.61	0.59	0.57	0.6	0.65	0.62
A-V	0.67	0.73	0.87	1.1	0.64	0.66	0.7	0.67	0.65	0.57

Table 1. *Cont.*

Number	BZ-Pcl-2-11	BZ-Pcl-2-12	BZ-Pcl-2-13	BZ-Pcl-2-14	BZ-Pcl-2-15	BZ-Pcl-2-16	BZ-Pcl-2-17	BZ-Pcl-2-18	BZ-Pcl-2-19	BZ-Pcl-2-20
Rock	Syenite facies I									
F	3.17	3.03	3.28	3.06	3.15	2.99	3.02	3.21	3.18	3.2
Na_2O	2.75	5.35	4.69	3.03	4.08	3.95	4.82	5.9	4.11	5.45
Ta_2O_5	1.53	1.78	1.81	1.15	1.76	1.55	0.97	1.81	1.68	0.29
SiO_2	1.28	0.75	0.53	2.69	0.5	1.06	0.7	0.86	0.48	1.36
Nb_2O_5	62.6	63	61.7	62.7	61.7	63.9	65	63.5	61.6	65.1
ThO_2	0.78	0.43	0.55	1.83	1.1	0.67	1.99	0.4	1.17	0.29
UO_2	11	10.7	9.89	10.5	10.3	11.4	6.33	6.79	10.2	7.79
CaO	8.41	8.27	8.4	7.8	8.41	8.7	8.16	8.35	8.39	9.01
TiO_2	4.03	4.35	3.66	4.51	4.22	4.04	4.3	4.21	4.21	4.41
La_2O_3	0.55	0.44	1.77	0.49	0.5	0.23	0.51	0.58	0.48	0.72
Ce_2O_3	1.77	1.69	1.55	1.79	2.43	1.21	2.84	2.45	2.41	1.31
Fe_2O_3	0.22	0.15	0.24	0.2	0.19	0.11	0.07	0.11	0.14	0.03
Total	98.11	99.91	98.08	99.71	98.28	99.80	98.67	98.13	98.08	98.97
Structural formula (∑B-site cations = 2)/apfu										
Na	0.32	0.63	0.57	0.34	0.49	0.46	0.56	0.69	0.5	0.62
Ca	0.54	0.54	0.57	0.48	0.56	0.56	0.52	0.54	0.56	0.57
La	0.01	0.01	0.04	0	0.01	0	0.01	0.01	0.01	0.02
Ce	0.04	0.04	0.04	0.04	0.06	0.03	0.06	0.05	0.06	0.03
Th	0.01	0	0	0.02	0.02	0	0.03	0.01	0.02	0
U	0.15	0.14	0.14	0.13	0.14	0.15	0.08	0.09	0.14	0.1
∑A	1.08	1.36	1.35	1.01	1.28	1.2	1.26	1.39	1.28	1.33
Nb	1.71	1.73	1.75	1.62	1.73	1.73	1.75	1.73	1.74	1.73
Ta	0.03	0.03	0.03	0.02	0.03	0.03	0.02	0.03	0.03	0
Ti	0.18	0.2	0.17	0.19	0.2	0.18	0.19	0.19	0.2	0.19
Si	0.08	0.05	0.03	0.15	0.03	0.06	0.04	0.05	0.03	0.08
Fe	0.01	0	0.01	0.01	0.01	0	0	0	0.01	0
∑B	2	2	2	2	2	2	2	2	2	2
F=O	0.6	0.58	0.65	0.56	0.62	0.57	0.57	0.61	0.63	0.59
A-V	0.92	0.64	0.65	0.99	0.72	0.8	0.74	0.61	0.72	0.67

Table 1. *Cont.*

Number	BZ-Pcl-3-1	BZ-Pcl-3-2	BZ-Pcl-3-3	BZ-Pcl-3-4	BZ-Pcl-3-5	BZ-Pcl-3-6	BZ-Pcl-3-7	BZ-Pcl-3-8	BZ-Pcl-3-9	BZ-Pcl-3-10
Rock	Syenite facies II									
F	3.01	3.22	3.08	3.29	3.31	2.86	4.21	3.18	3.11	3.11
Na_2O	5.45	6.91	6.34	6.28	5.28	6.39	4.57	6.19	6.19	6.21
Ta_2O_5	0.64	0.85	0.91	0.86	1.14	1.77	1.89	0.62	1.52	1.28
SiO_2	0.88	0.69	1.33	1.01	1.03	1.08	0.87	1.12	0.49	0.51
Nb_2O_5	64.9	65.8	67.1	67.3	65.9	65.1	67.9	66.8	65.8	66.6
ThO_2	1.88	1.02	0.31	0.61	1.12	1.38	0.83	1.21	1.41	0.79
UO_2	7.02	5.83	8.11	7.61	6.41	6.11	6.49	5.19	5.62	5.46
CaO	1.28	1.61	1.17	1.31	1.52	1.41	1.25	1.48	1.52	1.69
TiO_2	2.72	2.81	2.41	2.61	2.38	2.89	2.71	2.86	2.86	2.63
La_2O_3	2.01	2.12	1.22	0.77	1.68	2.35	0.62	2.11	1.19	1.95
Ce_2O_3	8.44	7.85	6.35	7.87	8.24	8.48	7.29	8.29	8.01	8.53
Fe_2O_3	0.11	0.13	0.16	0.08	0.25	0.02	0.03	0.01	0.36	0.14
Total	98.34	98.86	98.51	99.55	98.24	99.86	98.63	99.01	98.11	98.89
Structural formula (∑B-site cations = 2)/apfu										
Na	0.65	0.82	0.73	0.72	0.62	0.75	0.52	0.71	0.73	0.73
Ca	0.08	0.11	0.07	0.08	0.1	0.09	0.08	0.09	0.1	0.11
La	0.05	0.05	0.03	0.02	0.04	0.05	0.01	0.05	0.03	0.04
Ce	0.19	0.18	0.14	0.17	0.18	0.19	0.16	0.18	0.18	0.19
Th	0.03	0.01	0	0	0.02	0.02	0	0.02	0.02	0.01
U	0.1	0.08	0.11	0.1	0.09	0.08	0.08	0.07	0.08	0.07
∑A	1.1	1.24	1.07	1.1	1.04	1.18	0.85	1.12	1.12	1.16
Nb	1.81	1.81	1.79	1.81	1.8	1.77	1.8	1.8	1.8	1.82
Ta	0.01	0.01	0.01	0.01	0.02	0.03	0.03	0.01	0.02	0.02
Ti	0.13	0.13	0.11	0.12	0.11	0.13	0.12	0.13	0.13	0.12
Si	0.05	0.04	0.08	0.06	0.06	0.07	0.05	0.07	0.03	0.03
Fe	0	0	0.01	0	0.01	0	0	0	0.02	0.01
∑B	2	2	2	2	2	2	2	2	2	2
F=O	0.59	0.62	0.58	0.62	0.63	0.55	0.78	0.6	0.59	0.6
A-V	0.9	0.76	0.93	0.9	0.96	0.82	1.15	0.88	0.88	0.84

Table 1. *Cont.*

Number	BZ-Pcl-3-11	BZ-Pcl-3-12	BZ-Pcl-3-13	BZ-Pcl-3-14	BZ-Pcl-3-15	BZ-Pcl-3-16	BZ-Pcl-3-17	BZ-Pcl-3-18	BZ-Pcl-3-19	BZ-Pcl-3-20
Rock	Syenite facies II									
F	3.22	3.21	3.12	3.13	3.01	3.08	3.19	3.25	3.33	3.15
Na_2O	5.49	4.24	4.21	5.49	5.98	5.63	5.52	6.24	5.3	6.38
Ta_2O_5	1.41	1.13	0.98	1.52	0.93	0.71	1.38	0.6	1.12	0.92
SiO_2	0.52	0.83	1.1	0.81	0.57	1.18	0.61	1.11	1.01	1.28
Nb_2O_5	65.3	67.6	67.6	66.9	65.7	66.6	65.3	66.8	65.9	67.2
ThO_2	0.68	1.22	0.12	0.41	1.66	0.11	0.6	1.23	1.16	0.37
UO_2	6.21	6.81	8.61	6.98	7.36	8.37	6.3	5.21	6.44	8.12
CaO	1.78	1.52	1.42	1.47	1.51	1.42	1.82	1.53	1.5	1.2
TiO_2	2.71	2.63	2.22	2.86	2.53	2.81	2.73	2.8	2.41	2.5
La_2O_3	2.59	1.69	1.19	1.69	2.11	1.78	2.57	2.23	1.7	1.31
Ce_2O_3	8.41	7.63	7.63	8.01	7.68	7.32	8.39	8.31	8.31	6.34
Fe_2O_3	0.18	0.07	0.09	0.14	0.12	0.23	0.14	0.11	0.26	0.18
Total	98.48	98.59	98.30	99.37	99.15	99.20	98.56	99.42	98.44	98.94
Structural formula (∑B-site cations)/apfu										
Na	0.65	0.49	0.49	0.63	0.71	0.65	0.66	0.72	0.62	0.73
Ca	0.12	0.1	0.09	0.09	0.1	0.09	0.12	0.1	0.1	0.08
La	0.06	0.04	0.03	0.04	0.05	0.04	0.06	0.05	0.04	0.03
Ce	0.19	0.17	0.17	0.17	0.17	0.16	0.19	0.18	0.18	0.14
Th	0.01	0.02	0	0.01	0.02	0	0.01	0.02	0.02	0
U	0.08	0.09	0.11	0.09	0.1	0.11	0.09	0.07	0.09	0.11
∑A	1.11	0.89	0.88	1.03	1.16	1.05	1.12	1.13	1.04	1.08
Nb	1.81	1.81	1.82	1.79	1.83	1.78	1.81	1.8	1.8	1.79
Ta	0.02	0.02	0.02	0.02	0.02	0.01	0.02	0.01	0.02	0.01
Ti	0.13	0.12	0.1	0.13	0.12	0.13	0.13	0.13	0.11	0.11
Si	0.03	0.05	0.07	0.05	0.04	0.07	0.04	0.07	0.06	0.08
Fe	0.01	0	0	0.01	0.01	0.01	0.01	0	0.01	0.01
∑B	2	2	2	2	2	2	2	2	2	2
F=O	0.63	0.6	0.59	0.59	0.59	0.58	0.62	0.61	0.64	0.59
A-V	0.89	1.11	1.12	0.97	0.84	0.95	0.88	0.87	0.96	0.92

Pyrochlore supergroup minerals contain various types of elements. We analyzed the main elements, not trace elements (Pb, Nd, Sn, Sb, Y, Mg, Mn and W). The trace elements test (Table 2) was found to indicate a certain amount of Pb, Nd, Sn and W, and their combined oxide content can reach 1–2 wt.%. Therefore, the oxide content totals in this table are somewhat low.

Table 2. Trace element content of pyrochlore supergroup minerals from the Boziguoer deposit.

Sample No.	BZ-Pcl-1-1	BZ-Pcl-1-2	BZ-Pcl-1-3	BZ-Pcl-1-4	BZ-Pcl-1-5	BZ-Pcl-1-6	BZ-Pcl-1-7	BZ-Pcl-1-8	BZ-Pcl-1-9	BZ-Pcl-1-10
Rock	Alkalic granite facies									
Li	35.1	39.8	32.6	14.0	11.4	23.3	25.9	6.6	7.7	10.3
Sc	0.19	0.26	0.10	0.09	0.12	0.07	0.34	0.33	0.16	0.25
V	0.02	0.05	0.02	0.00	0.00	0.01	0.13	0.03	0.04	0.19
Cr	15.7	2.88	1.10	3.52	2.12	14.7	25.7	3.37	2.94	11.7
Co	0.04	0.09	0.11	0.06	0.06	0.00	0.07	0.06	0.05	0.05
Ni	0.14	0.00	0.00	0.00	0.10	0.17	0.32	0.00	0.23	0.00
Cu	7.13	1.88	1.53	1.08	1.15	1.26	3.10	2.07	0.97	6.21
Zn	177	80.1	30.2	6.00	39.2	32.6	316	10,630	147	37,803
Ga	363	342	310	298	305	328	273	228	326	317
Ge	136	122	109	107	113	114	77.4	79.9	105	103
Rb	3.27	7.22	3.34	1.40	2.80	4.49	5.18	13.37	2.26	4.39
Sr	633	624	678	654	672	682	370	360	366	403
Y	3941	1940	1507	1615	2365	2173	436	450	543	918
Zr	131	287	104	127	94.6	99.0	245	375	227	266
Nb	389,676	400,247	401,359	403,532	399,678	397,061	375,443	380,754	381,211	373,589
Mo	101	55.7	105	117	111	109	6.69	6.68	7.04	7.98
Sn	881	978	847	889	906	896	587	858	663	669
Cs	2.84	8.47	2.12	1.41	4.02	2.05	4.52	6.86	4.72	6.81
Ba	10.8	12.8	6.82	7.70	10.37	9.75	13.0	13.7	16.4	15.7
La	6405	5579	5035	4577	4988	6158	3741	3182	5603	4970
Ce	19,180	18,641	17,263	16,656	17,600	19,742	11,241	10,755	16,507	15,954
Pr	2152	2056	1905	1895	1981	2167	1208	1240	1814	1813
Nd	7717	7103	6569	6559	7057	7448	3714	4080	5652	5818
Sm	1323	1126	1019	1065	1138	1167	656	781	1030	1139
Eu	45.8	38.3	32.7	34.5	38.3	39.0	17.8	19.4	28.6	31.9
Gd	648	443	405	413	476	473	324	386	511	628
Tb	118	73.6	65.8	70.2	81.0	79.9	47.6	56.2	75.6	101
Dy	691	384	348	377	434	427	245	279	371	537
Ho	119	58.2	53.0	57.0	66.2	65.9	32.6	37.8	46.5	73.6
Er	389	181	159	175	204	203	86.8	101	110	183
Tm	42.6	20.2	15.8	18.9	22.8	22.7	7.16	9.52	8.64	15.8
Yb	223	109	75.5	97.4	133	129	36.1	55.6	41.5	87.0

Table 2. *Cont.*

Sample No.	BZ-Pcl-1-1	BZ-Pcl-1-2	BZ-Pcl-1-3	BZ-Pcl-1-4	BZ-Pcl-1-5	BZ-Pcl-1-6	BZ-Pcl-1-7	BZ-Pcl-1-8	BZ-Pcl-1-9	BZ-Pcl-1-10
Rock	Alkalic granite facies									
Lu	15.9	7.20	4.68	5.88	9.07	8.79	2.17	4.08	2.75	6.60
Hf	26.1	55.9	14.1	13.0	13.9	15.4	12.9	45.0	40.3	15.4
Ta	17,697	14,000	15,515	14,185	18,652	17,988	22,845	26,340	27,933	24,964
W	1181	1221	1672	1782	1712	1648	1421	817	774	1033
Pb	14,318	13,586	13,837	13,813	14,616	15,501	9880	8655	3635	9387
Th	7261	8252	6071	6238	6754	6821	5190	6444	7563	7306
U	36,824	37,371	37,956	38,009	37,605	38,937	71,851	82,542	77,461	73,864
Sample No.	**BZ-Pcl-2-1**	**BZ-Pcl-2-2**	**BZ-Pcl-2-3**	**BZ-Pcl-2-4**	**BZ-Pcl-2-5**	**BZ-Pcl-3-1**	**BZ-Pcl-3-2**	**BZ-Pcl-3-3**	**BZ-Pcl-3-4**	**BZ-Pcl-3-5**
Rock	Syenite facies I					Syenite facies II				
Li	34.4	51.6	66.1	20.2	31.2	51.1	63.2	47.5	52.1	77.3
Sc	0.21	0.16	0.30	0.29	0.18	0.37	0.31	0.43	0.24	0.33
V	0.00	0.01	0.02	0.00	0.00	0.01	0.03	0.03	0.02	0.10
Cr	13.2	3.74	2.13	3.78	5.22	12.1	15.1	2.48	3.74	5.27
Co	0.02	0.03	0.01	0.02	0.01	0.01	0.02	0.03	0.05	0.02
Ni	0.04	0.00	0.00	0.00	0.10	0.12	0.11	0.05	0.25	0.02
Cu	6.15	2.74	2.51	3.08	2.11	1.75	4.22	2.11	3.92	5.10
Zn	148	225	78.2	97.8	55.2	74.5	92.3	102	113	97.5
Ga	452	551	432	392	351	312	492	531	520	602
Ge	155	172	121	112	102	131	120	122	151	136
Rb	4.78	5.12	4.42	3.21	2.53	4.47	5.98	6.36	7.31	9.91
Sr	733	701	698	722	688	680	751	721	702	822
Y	4731	2331	1811	1623	2374	5920	2925	2257	3261	825
Zr	313	298	253	320	253	234	322	407	351	382
Nb	432,610	422,876	446,103	417,105	423,114	454,584	463,879	466,448	435,879	443,567
Mo	74.3	58.5	67.2	74.5	120	113	130	122	151	102
Sn	992	956	1022	1113	985	898	1123	1102	988	1223
Cs	7.54	6.32	4.42	5.31	3.31	9.11	5.32	6.97	5.35	6.51
Ba	9.31	6.21	5.32	8.32	5.55	9.32	11.2	12.3	9.32	6.51
La	7663	6591	6112	4587	5003	9612	8367	7555	9229	8406
Ce	22,451	22,301	20,645	16,632	17,606	28,763	27,955	25,887	29,605	24,763

Table 2. *Cont.*

Sample No.	BZ-Pcl-2-1	BZ-Pcl-2-2	BZ-Pcl-2-3	BZ-Pcl-2-4	BZ-Pcl-2-5	BZ-Pcl-3-1	BZ-Pcl-3-2	BZ-Pcl-3-3	BZ-Pcl-3-4	BZ-Pcl-3-5
Rock			Syenite facies I					Syenite facies II		
Pr	2553	2451	2261	1884	2003	3215	3101	2865	3248	2725
Nd	9221	8496	7854	6498	7101	11,548	10,631	9854	11,169	8479
Sm	1573	1311	1219	1082	1205	1993	1679	1530	1748	1548
Eu	56.3	44.1	39.1	35.6	41.2	70.1	58.1	49.2	59.3	43.1
Gd	781	529	479	402	485	975	659	608	711	768
Tb	143	89.1	80.1	69.5	90.2	172	111	99.1	118	115
Dy	830	468	409	396	441	1056	579	524	638	561
Ho	142	71.2	62.9	59.3	65.3	181	87.5	80.2	97.9	70.1
Er	471	220	189	181	213	589	272.3	241	306	163
Tm	53.2	26.3	19.1	19.6	23.5	65.1	31.2	24.2	33.9	13.1
Yb	271	128	92.1	99.1	143	329	162.9	115	192	61.9
Lu	19.1	8.53	5.9	6.21	10.2	24.1	11.1	7.14	13.4	3.92
Hf	53.3	58.9	31.2	47.5	44.3	52.1	31.2	58.8	61.1	33.5
Ta	13,444	13,105	15,964	19,104	20,486	8101	7543	9203	10,778	11,541
W	1271	1253	1544	1631	1692	1754	1812	1815	1765	1475
Pb	11,534	10,531	11,157	12,548	12,154	13,521	13,022	14,554	15,658	14,987
Th	6657	6895	7458	8143	8025	5103	8013	7485	7985	6921
U	74,654	73,551	69,531	86,698	102,598	105,874	78,546	69,854	72,454	68,589

In all three lithofacies, the pyrochlore supergroup mineral grains primarily show an octahedral morphology or form irregular granular aggregates with imperfect cleavage. They are yellow, dark red or reddish brown under plane polarized light, and grain sizes range from 70 to 140 μm. The pyrochlore supergroup mineral's grains are disseminated unevenly throughout other major minerals (Figure 4d–f), and as with other accessory phases, textural evidence indicates that they crystallized relatively late, after the crystallization of most other magmatic minerals, such as alkaline feldspars, quartz, arfvedsonite and aegirine.

4. Samples and Analytical Methods

We collected samples from three mineralized lithofacies and observed the texture and occurrence of the pyrochlore supergroup minerals using optical and scanning electron microscopy (SEM) combined with back-scattered electron (BSE) images. The major oxides of the pyrochlore supergroup minerals in alkalic granite facies, syenite facies I and syenite facies II were analyzed in 33, 20 and 20 grains, respectively. The trace element content was determined and compared to the trace element composition of the host rocks (previously published [17]).

Major oxide analysis was undertaken using wavelength-dispersive spectrometry on an EPMA-1600 electron probe at the Tianjin Geological Research Center, operating at an accelerating voltage of 15 kV with a 12 nA beam current, 5 μm beam, peak counting time of 20 s and background time of 10 s for major elements. A program based on the ZAF procedure was used for data reduction. Fe^{2+}–Fe^{3+} redistribution from electron microprobe analyses was carried out using the general equation of Droop (1987) [64] for estimating Fe^{3+}. The experimental results were corrected using ZAF, and the 1σ uncertainty was <10% when the element content was greater than 0.1 ppm.

Trace element abundance in the pyrochlore supergroup minerals was determined using laser ablation inductively coupled plasma mass spectrometry (LA–ICP–MS) applied to polished thick sections, at the In Situ Mineral Geochemistry Lab, Ore Deposit and Exploration Centre (ODEC), Hefei University of Technology, Hefei, Anhui Province, China. These analyses were undertaken using an Agilent 7900 Quadrupole ICP–MS coupled to a Photon Machines Analyte HE 193-nm ArF Excimer Laser Ablation system equipped with a SQUID signal smoothing device. Helium was used as carrier gas and mixed with Ar makeup gas via a T-connector before entering the ICP. Each analysis was performed at a spot diameter of 30 μm, laser pulse frequency of 8 Hz and with a laser energy of ~2 J cm^{-2} for 40 s after measuring a gas blank for 20 s. Standard reference glass materials GSE-1g, GSD-1g and BCR-2G were used as external standards to plot calibration curves using preferred element concentrations for the USGS reference glasses from the GeoReM database (http://georem.mpch-mainz.gwdg.de/. Accessed on 1 June 2022). Off-line data processing was undertaken using the ICPMS Data Cal software package [65], and trace element compositions of oxide minerals were calibrated against multiple reference materials using ^{57}Fe for internal standardization. The analytical uncertainty of the trace elements determined during this study is 10%.

5. Analytical Results

5.1. Major Element Composition of Pyrochlore

The pyrochlore supergroup mineral's general formula is $A_{2-m}B_{2\times 6-w}Y_{1-n}$ [31,66]. The A-site is occupied by large cations such as As, Ba, Bi, Ca, Cs, K, Mg, Mn, Na, Pb, REE, Sb, Sr, Th, U and Y. The CaO content of the Boziguoer pyrochlore supergroup minerals ranges from 10 to 16 wt.% in the alkalic granite facies, 7 to 9 wt.% in syenite facies I and 1.1 to 1.7 wt.% in syenite facies II (Table 1). The REE are mainly La and Ce, with La_2O_3 and Ce_2O_3 respectively ranging from 0.1 to 1.6 wt.% and 0.1 to 3.5 wt.% in the alkalic granite facies, 0 to 2 wt.% and 1 to 3.6 wt.% in syenite facies I and 0.5 to 2.6 wt.% and 6.4 to 8.5 wt.% in syenite facies II. There is little difference in Na_2O, ThO_2 and UO_2 content in the pyrochlore supergroup minerals from the three lithofacies.

The B-site accommodates smaller and highly charged cations such as Nb, Ta, Ti, Zr, Fe^{3+}, Al and Si [36] and rarely W^{5+} [67]. The Nb_2O_5 content varies from 53 to 60 wt.% in the alkalic granite facies, from 62 to 65 wt.% in syenite facies I and from 65 to 68 wt.% in syenite facies II. The TiO_2 content in the alkalic granite, syenite facies I and syenite facies II ranges from 5 to 8 wt.%, 4 to 5 wt.% and 2 to 3 wt.%, respectively. Most analyses yielded low content of Ta_2O_5, SiO_2 and Fe_2O_3 (Table 1).

The Y- and X-site anions can be O, OH and F. The F content in the three lithofacies varies from 1 to 2.4 wt.% in the alkalic granite facies, 3 to 3.6 wt.% in syenite facies I and 3 to 4.3 wt.% in syenite facies II.

The structural formula for the Boziguoer pyrochlore supergroup minerals has been calculated in terms of two cations in the B-site [68]. Vacancies are common in the A- and Y-sites. The calculated results show that the A-site has vacancies (A-V) varying from 0.05 to 0.96 apfu in the alkalic granite facies, 0.57 to 1.1 apfu in syenite facies I and 0.76 to 1.15 apfu in syenite facies II. There is a strong negative correlation between Nb and Ti, Ta and Ca (Figure 5a–c). Such trends indicate that substitution is Nb for Ti, Ta and Ca. There is a positive correlation between Nb and F, La + Ce and A vacancies, but Na and Nb are not correlated (not shown). The variation plot between substitution mechanisms (Figure 6) shows a trend with a slope of −1.0006, indicating that it can quantitatively describe the substitution mechanism of the pyrochlore supergroup minerals in the lithofacies at Boziguoer.

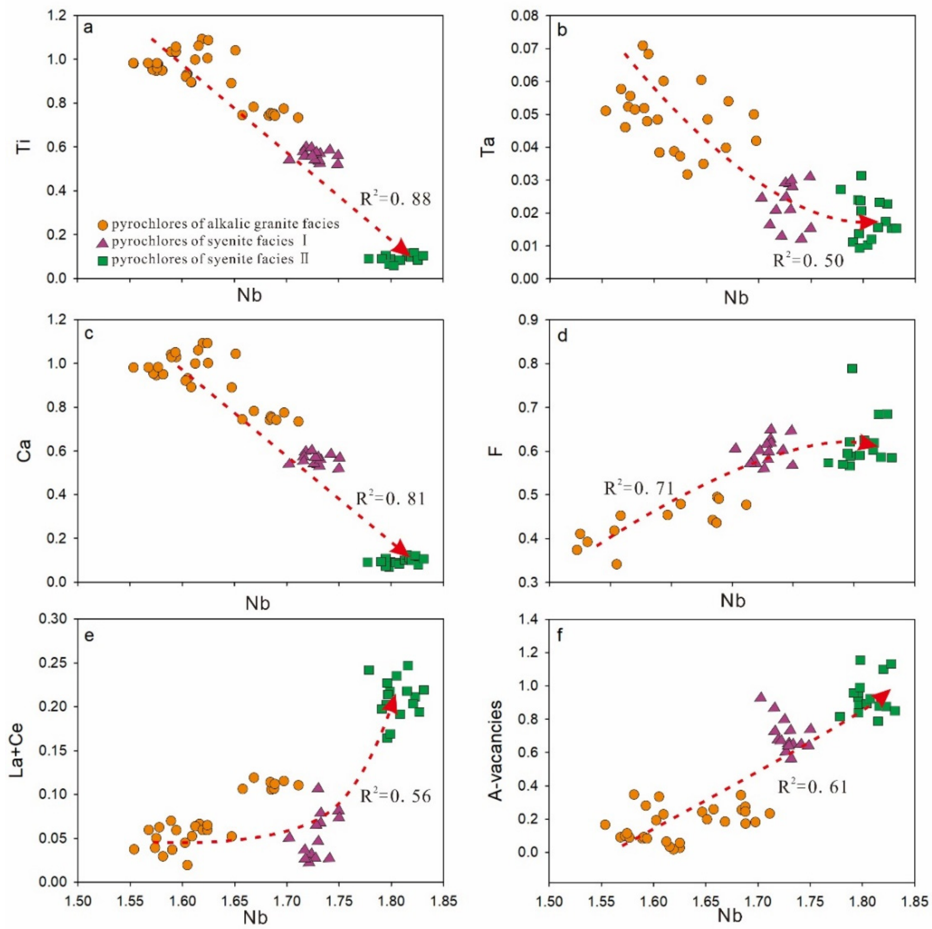

Figure 5. Variation in selected elements (apfu) in pyrochlore supergroup minerals from Boziguoer deposit. (**a**) Ti is negatively correlated with Nb, R^2 is 0.88; (**b**) Ta is negatively correlated with Nb, R^2 is 0.50; (**c**) Ca is negatively correlated with Nb, R^2 is 0.81; (**d**) F is positively correlated with Nb, R^2 is 0.71; (**e**) La+Ce is positively correlated with Nb, R^2 is 0.56; (**f**) A-vacancies is positively correlated with Nb, R^2 is 0.61.

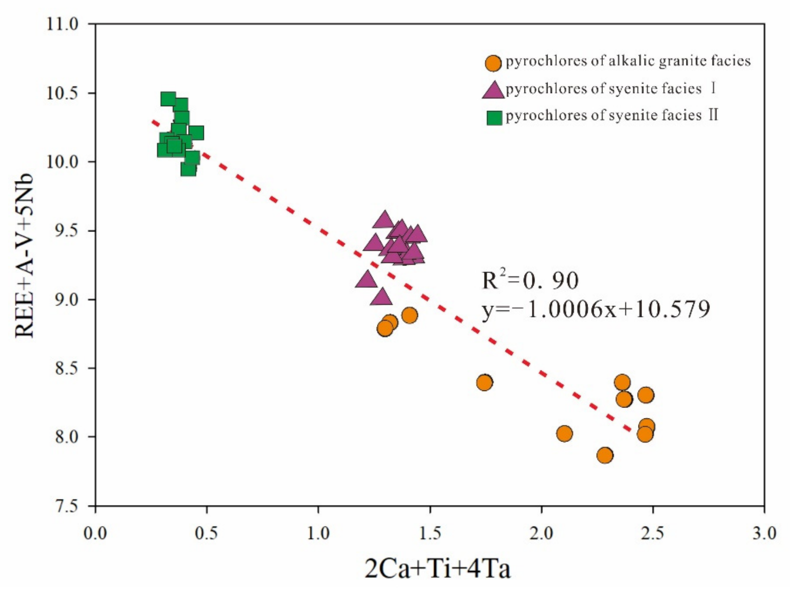

Figure 6. Variation in selected elements (apfu) in pyrochlore supergroup minerals from Boziguoer deposit.

5.2. Classification of Pyrochlore in the Boziguoer Deposit

The results show that the Boziguoer pyrochlore supergroup minerals belong to the general pyrochlore supergroup (Figure 7). Five types of pyrochlore group minerals (pyrochlore, microlite, roméite, betafite and elsmoreite) have been defined, based on the atomic proportion of B-site atoms Nb, Ta, Sb, Ti and W [66]. All varieties in the Boziguoer deposit belong to the pyrochlore type, with Ti varying within roughly the same range as that in pyrochlore supergroup minerals from pegmatites associated with alkali granites and albitized granites (Figure 7). They are also similar to pyrochlore supergroup minerals from nepheline syenites, which also have very low Ta concentrations (atomic Nb:Ta ratio ranges from 10 to 1000). The low Ta content is the most conspicuous geochemical difference between pyrochlore supergroup minerals in alkaline rocks and those from carbonatite and granite pegmatites (Figure 7).

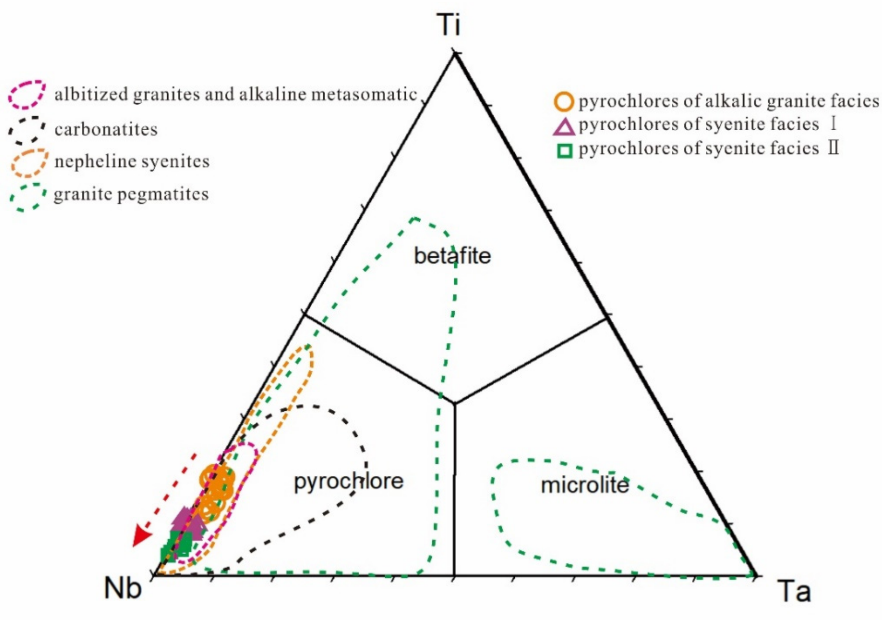

Figure 7. Triangular Nb–Ti–Ta pyrochlore classification scheme (modified by [30,40,66,69,70]).

Pyrochlore subgroup minerals are further classified based on the dominant valences at the A- and Y-sites [20,66]. In the Boziguoer deposit, the A-site in the pyrochlore supergroup minerals is occupied by Ca, Na and vacancies (Figure 8), while the Y-sites mainly host F anions (W_F/% is 0.71–4.21, the average is 2.56). Thus, fluorcalciopyrochlore, fluorkenopyrochlore and fluornatropyrochlore were identified in Boziguoer. The pyrochlore supergroup minerals in the alkalic granite facies are mainly fluorcalciopyrochlore, with a small amount of fluornatropyrochlore. Syenite facies I and syenite facies II mainly contain fluorkenopyrochlore, and the syenite facies II grains have more A-site vacancies and higher Na/Ca than those from syenite facies I (Figure 8).

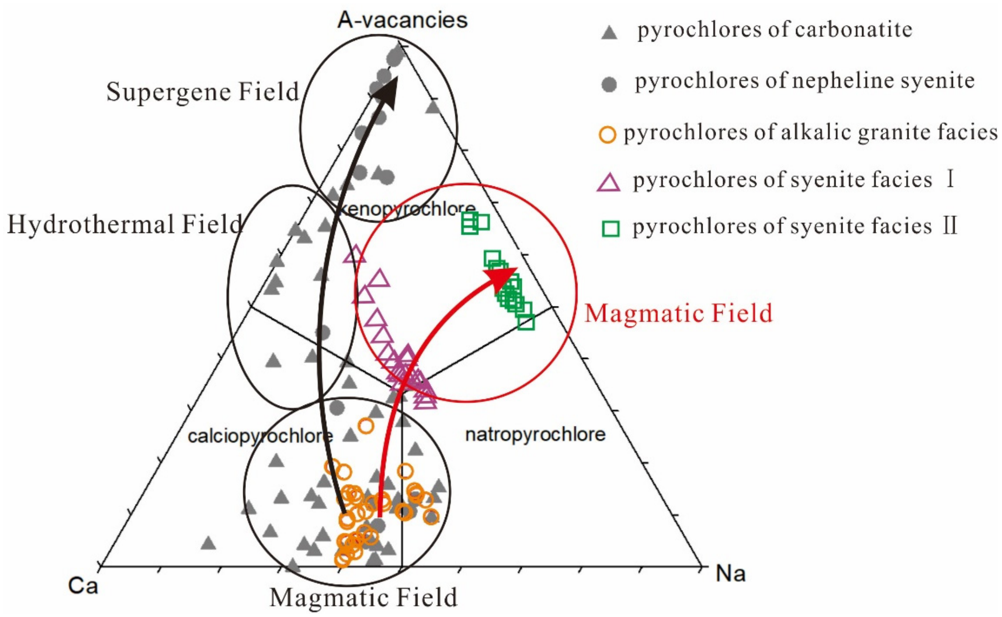

Figure 8. Ternary plot of Ca, Na and A-site vacancy (modified from [36]). The magmatic, hydrothermal and supergene fields of pyrochlore supergroup minerals (black circles) are from [36]. The black arrow indicates the compositional evolution of pyrochlore supergroup minerals from carbonatite. The magmatic field of pyrochlore supergroup minerals from the Boziguoer deposit (red circle) is proposed based on the results presented in this study. The red arrow indicates their compositional evolution. The pyrochlore supergroup mineral data for carbonatite are from [23,31,37,41]; data for nepheline syenite are from [35].

5.3. Trace Element Composition of Pyrochlore

Trace element data for Boziguoer pyrochlore supergroup minerals are given in Table 2. The primitive mantle-normalized trace element and chondrite-normalized REE patterns are similar to those of the host rock (Figure 9), displaying negative large ion lithophile element (LILE; Rb, Sr and Ba) anomalies, and positive high-field-strength element (HFSE) and light rare earth element (LREE) anomalies. Negative Eu anomalies occur in both the minerals and host rock, but the normalized total trace element and total REE element content in the pyrochlore supergroup minerals is higher than that in the host rock. Rb and Ba are more depleted in pyrochlore supergroup minerals than in the host rock, but contains more U, Th, Nb and Ta. The REE and trace element distribution characteristics of the three lithofacies are roughly consistent. However, the total amount of REE and trace elements in the two syenite facies is slightly higher than that in the alkalic granite facies rocks.

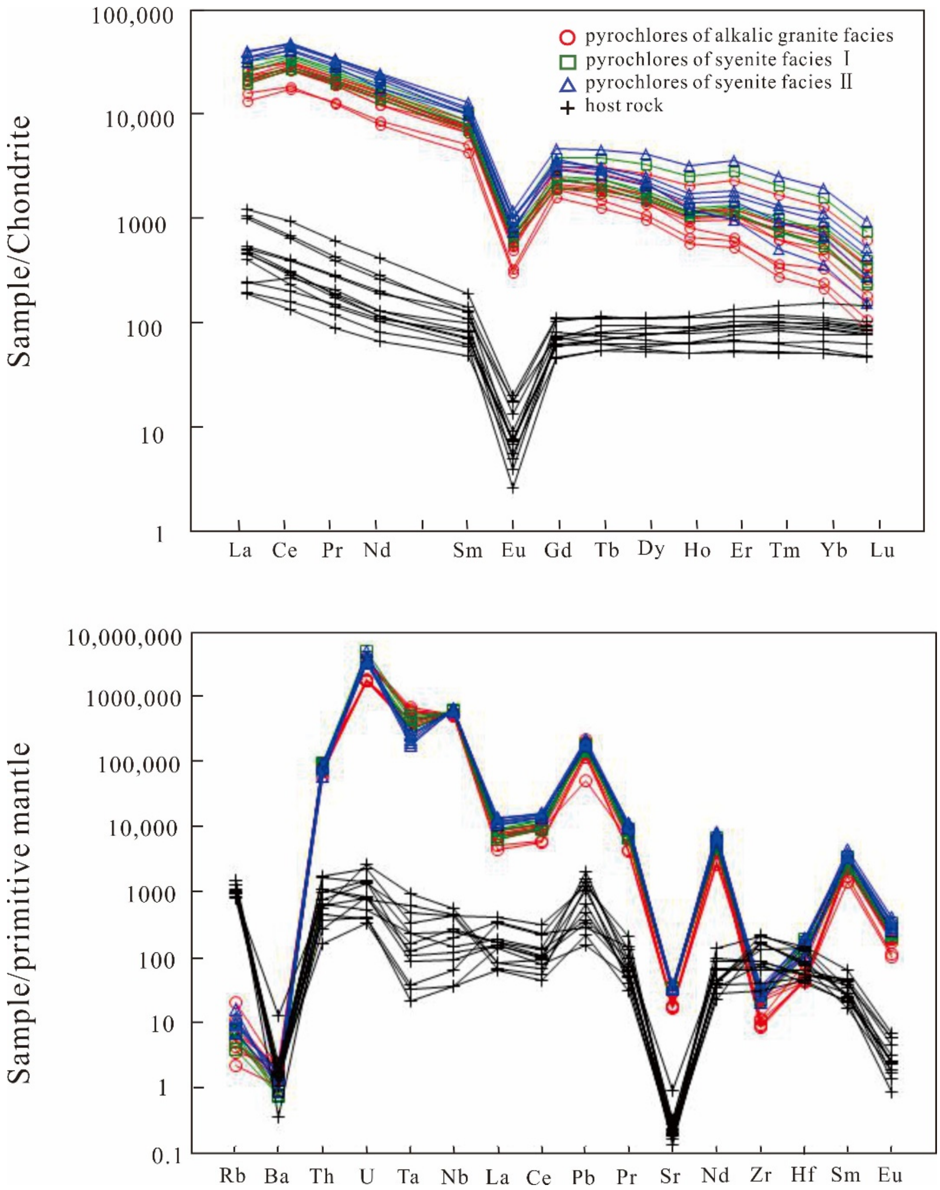

Figure 9. Chondrite-normalized REE patterns and primitive mantle-normalized trace element patterns for Boziguoer pyrochlore supergroup minerals and the host rock. The chondrite and primitive mantle values are from [71].

6. Discussion

6.1. Substitution of Elements in Pyrochlore Supergroup Minerals

There are several elemental substitution mechanisms established for the pyrochlore supergroup minerals from carbonatite and nepheline syenite [25,32,33,37,38,68,72–77]; however, there are few studies on the pyrochlore supergroup minerals in alkaline felsic rocks. The substitution of elements in the Boziguoer pyrochlore supergroup minerals involves the new mineral, fluornatropyrochlore. Therefore, it is worth comparing the substitution mechanisms in the pyrochlore supergroup minerals from Boziguoer with that from other rock types.

During magmatic evolution, the pyrochlore supergroup minerals from carbonatite become progressively enriched in Na, Ca, F and Nb and depleted in Ta, Th, REE, Ti and U [33,37]. Therefore, the pyrochlore supergroup minerals' Nb/Ta ratio in carbonatite increases with the degree of magmatic evolution. Similarly, pyrochlore supergroup minerals from Boziguoer are enriched in Nb and F and depleted in Ta and Ti with magmatic evolution.

However, there is a difference between Boziguoer and carbonatite pyrochlore supergroup minerals with respect to the elements occupying the A-site. Pyrochlore supergroup minerals from carbonatites from the Lueshe, Niocan and Bond Zone, as well as nepheline syenite from the Lovozero, plot in all three fields on a Ca-Na-A vacancy ternary plot: magmatic, hydrothermal and supergene (Figure 8). The compositional evolution from calciopyrochlore and natropyrochlore toward kenopyrochlore (black arrow in Figure 8) is related to the exchange of Ba (Rb, Sr) for Ca+ Na and the consequent vacancy in the A-site [34,36]. Similar trends can be found in the Bingo pyrochlore supergroup minerals [32], which are a product of weathering, and in those from the Kola carbonatites [73], derived from supergene or low-temperature hydrothermal alteration. At Boziguoer, the trend from calciopyrochlore and natropyrochlore toward kenopyrochlore (red arrow in Figure 8) is related to the exchange of REE (La, Ce) for Ca, and the consequent vacancy in the A-site (Figure 6). Therefore, an evolutionary trend for the pyrochlore supergroup minerals crystallized from the Boziguoer alkaline felsic magma can be defined (red arrow to red circle in Figure 8). This compositional evolution is in contrast to that defined for the pyrochlore supergroup minerals crystallized from carbonatites and nepheline syenites. During magmatic evolution at Boziguoer, the variation in elements in the pyrochlore supergroup minerals changed as follows: B-site—Nb increased, Ti and Ta decreased; A-site—Ca decreased, La + Ce and A vacancies increased. Given this substitution of elements in the pyrochlore supergroup minerals during Boziguoer magma evolution controlled by the A- and B-sites, and on the basis of maintaining the charge balance (Figure 7), we propose the following substitution mechanism:

$$2Ca^{2+} + Ti^{4+} + 4Ta^{5+} = REE^{3+} + \text{A-V} + 5Nb^{5+}$$

6.2. Genesis of Pyrochlore Supergroup Minerals from the Boziguoer Deposit

The pyrochlore supergroup minerals can form either by crystallization from a magma or during hydrothermal alteration. Magmatic pyrochlore supergroup minerals occur in pyroxenite, calcite carbonatite, silicate xenoliths and syenite. Hydrothermal pyrochlore supergroup minerals occur in hydrothermal veins within the complex, whereas supergene pyrochlore supergroup minerals accumulate within the lateritic profile [34]. The pyrochlore supergroup minerals in the Boziguoer alkaline complex is disseminated, rather than intergrown with hydrothermal veins and in the lateritic profile. Thus, the pyrochlore supergroup minerals in the Boziguoer deposit are likely a magmatic product. Their chemical composition also indicates a magmatic origin, as outlined below.

Firstly, Lumpkin and Ewing (1995) [31] argued that A-site large cations can be useful for the identification of chemical variation in pyrochlore supergroup minerals because these large cations are related to host rock evolution and alteration. LILEs are highly active elements and their content increases with fluid participation. The pyrochlore supergroup minerals' LILE content at Boziguoer is extremely low, with the primitive mantle-normalized trace element plot showing negative anomalies of LILE (K, Sr and Ba) (Figure 9), and the results of EPMA tests were all below the detection limit, but the pyrochlore supergroup minerals LILE of hydrothermal deposits can reach 0.71 apfu of Sr, 0.48 apfu of Ba and 0.19 apfu of K [78]. These characteristics suggest that the degree of fluid activity was extremely low.

Secondly, while pyrochlore supergroup minerals are generally enriched in REE, and REE partition coefficients suggest that the LREE are more compatible than HREE [79]. This explains the high REE concentration with the enrichment of LREE in naturally occurring magmatic pyrochlore supergroup minerals. The pyrochlore supergroup minerals in Boziguoer (Figure 9) display enrichment in LREE, indicating a magmatic origin. Moreover, their primitive mantle-normalized trace element and chondrite-normalized REE patterns are similar to those of their host rocks (Figure 9), indicating that the studied pyrochlore supergroup minerals were the product of magmatic crystallization.

Thirdly, the pyrochlore supergroup minerals are able to strongly fractionate trace elements during magmatic evolution. They efficiently fractionate Zr from Hf and Nb from Ta, according to the differences among D_{Zr}, D_{Hf}, D_{Nb} and D_{Ta} [79]. The Boziguoer pyrochlore supergroup minerals feature positive anomalies of Nb and Ta, and negative anomalies of Zr and Hf, which are not seen in the host rock. These fractionations provide further evidence that the Boziguoer pyrochlore supergroup minerals are magmatic in origin.

The conditions of crystallization can be discerned from the pyrochlore supergroup minerals' composition. Under oxidizing conditions, D_{Th} is higher than the corresponding D_U, resulting in U and Th fractionation in silicate magmas [79]. The content of U and Th in the host rock at Boziguoer is similar, indicating that the concentrations of those elements in the magma were similar when the pyrochlore supergroup minerals crystallized. However, the latter are enriched in U over Th (Figure 9), indicating that that the magma was also somewhat reduced at the time of the pyrochlore supergroup minerals' crystallization.

Compared with the host rocks, the pyrochlore supergroup minerals' REE pattern has a tetrad effect. Figure 10 shows the τ coefficients of the pyrochlore supergroup minerals and their host rocks. The calculation method of τ coefficients is derived from [80], where τ is each of the four tetrad coefficients, with positive values indicating a negative parabola, i.e., a ridge, or M-type tetrad, and negative values indicating a positive parabola, i.e., a trough, or W-type tetrad. The tetrad behavior is clear in the pyrochlore supergroup minerals but less clear in host rocks. It indicates that the magma may have undergone sufficient differentiation when the pyrochlore supergroup minerals crystallized. The LREE tetrads, $\tau 1$ and $\tau 2$, are strongly positive in all pyrochlore supergroup minerals. One possibility is that LREE was gradually enriched in the residual magma.

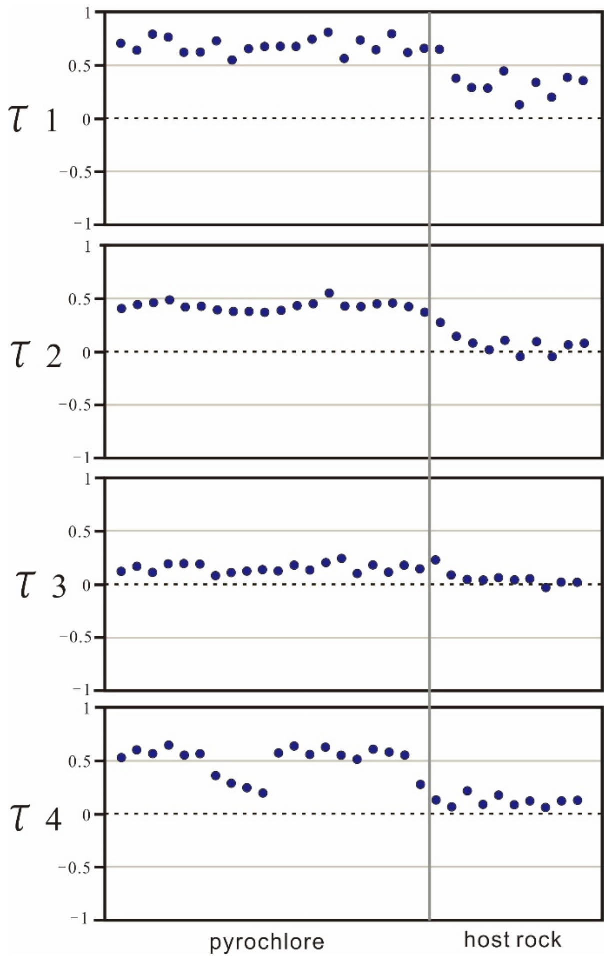

Figure 10. Tetrad τ coefficients for pyrochlore supergroup minerals and their host rocks. The first to fourth tetrad coefficients are shown, respectively.

6.3. Implications for Alkaline Magma Differentiation and Nb Enrichment

In carbonatitic and alkaline magma systems, Nb is more soluble than Ta [81], which could explain the occurrence of Ta-rich pyrochlore supergroup minerals in primitive magmas and Nb-rich, Ta-poor pyrochlore supergroup minerals in more evolved, late-stage magmas. The pyrochlore supergroup minerals in the Boziguoer deposit are Nb-rich and Ta-poor, suggesting a relatively high degree of evolution for the ore-bearing rocks. Moreover, progressing from the alkalic granite facies to syenite facies I and then to syenite facies II, pyrochlore supergroup minerals evolve towards the Nb-rich pyrochlore end-member (Figure 7). On the other hand, the total amount of REE in the two syenite facies is slightly higher than that in the alkalic granite facies (Figure 9), even though the latter is less evolved. Our previous study of aegirine and arfvedsonite from Boziguoer also shows the same evolutionary trend [30], in contrast to the trend seen in calc-alkaline rocks, where the degree of evolution of granite facies is generally higher than that of syenite, monzonite and anorthosite facies. The dark minerals in Boziguoer are aegirine and arfvedsonite, which are likely products of late magmatic evolution [82–84]. The Bowen reaction sequence also indicates that dark alkaline minerals in alkaline rocks usually crystallize later than feldspar and quartz. This, combined with petrographic observations (Figure 4b,c), suggests that the sequence of crystallization of the main minerals in Boziguoer is from albite, K-feldspar and quartz, to aegirine and arfvedsonite. Syenite facies II has the highest content of arfvedsonite and aegirine, indicating that it was the latest and most evolved lithofacies. The alkalic granite facies has the least amount of arfvedsonite and aegirine, placing it first in the evolutionary sequence. The most advanced lithofacies have the most evolved pyrochlore supergroup minerals with the highest Nb content, suggesting that Nb in these minerals can indicate the degree of magmatic evolution, and that fractional crystallization is likely the key mechanism controlling the difference in pyrochlore supergroup minerals composition in different lithofacies of the Boziguoer deposit.

7. Conclusions

The disseminated pyrochlore supergroup minerals in the Boziguoer deposit can be classified as fluornatropyrochlore, fluorcalciopyrochlore and fluorkenopyrochlore. They are enriched in Nb and depleted in Ta, with extremely low content of LILE.

A new substitution mechanism for the pyrochlore supergroup minerals is proposed based on the association between Ti, Ta and Ca, and the Nb, La + Ce and A vacancies, i.e., $2Ca^{2+} + Ti^{4+} + 4Ta^{5+} = REE^{3+} + A\text{-}V + 5Nb^{5+}$.

The sequence of crystallization for the main minerals in the Boziguoer deposit is albite + K-feldspar + quartz $\rightarrow$ aegirine + arfvedsonite $\rightarrow$ pyrochlore supergroup minerals. The content of Nb in the pyrochlore supergroup minerals is likely associated with magmatic evolution. The content of Nb, Ta, Zr and Hf in the pyrochlore supergroup minerals and their host rocks suggests that pyrochlore supergroup minerals fractionation may cause a decoupling between Nb and Ta and between Zr and Hf.

There is a significant difference between the elements hosted in the A-site of the pyrochlore supergroup minerals from Boziguoer alkaline rocks and that from other rocks (e.g., carbonatite and nepheline syenite). The substitution of Ba (Rb, Sr) for the Ca+ Na + vacancy in pyrochlore supergroup minerals from carbonatite and nepheline syenite is related to hydrothermal and supergene processes, whereas the replacement of REE (La, Ce) with the Ca + vacancy in the pyrochlore supergroup minerals from the Boziguoer deposit is likely related to alkaline magma evolution.

Supplementary Materials: The following supporting information can be downloaded at: https://www.mdpi.com/article/10.3390/min12070785/s1, Table S1. Trace element content of astrophyllite from the Boziguoer deposit.

Author Contributions: Conceptualization, Z.S. and K.Q.; field investigation, Z.S and K.Q.; methodology, Y.M.; software, F.W.; validation, Y.M., D.T. and Q.Z.; resources, K.Q.; data curation, Z.S.; writing—original draft preparation, Z.S.; writing—review and editing, K.Q. and N.J.E.; visualization, Y.M. and D.T.; supervision, K.Q.; funding acquisition, K.Q. All authors have read and agreed to the published version of the manuscript.

Funding: This research was financially supported by the National Natural Science Foundation of China (41830430), the Second Tibetan Plateau Scientific Expedition and Research Program (STEP, Grant No. 2019QZKK0806) and the Key Deployment Project of CAS (ZDRW-ZS-2020-4-1).

Data Availability Statement: Not applicable.

Acknowledgments: Geological Engineers Decheng Ma, Chen Li and Xianfeng Wei from the 701 Geological Team of Xinjiang Nonferrous Geoexploration Bureau provided valuable assistance in the field survey. Senior engineer Haiming Xu from the Chinese Academy of Geological Sciences introduced the local situation and guide. We are also grateful to Hu Guo at Tianjin Geological Research Center for the EPMA analysis.

Conflicts of Interest: The authors declare no conflict of interest.

References

1. Wang, D.H.; Wang, R.J.; Li, J.K.; Zhao, Z.; Yu, Y.; Dai, J.J.; Chen, Z.H.; Li, D.X.; Qu, W.J.; Deng, M.C.; et al. The progress in the strategic research and survey of rare earth, rare metal and rare-scattered elements mineral resources. *Geol. China* **2013**, *40*, 361–370. (In Chinese with English Abstract)
2. Zhai, M.G.; Wu, F.Y.; Hu, R.Z.; Jiang, S.Y.; Li, W.C.; Wang, R.C.; Wang, D.H.; Qi, T.; Qin, K.Z.; Wen, H.J. Critical metal mineral resources: Current research status and scientific issues. *Bull. Natl. Nat. Sci. Found. China* **2019**, *2*, 106–111. (In Chinese with English Abstract)
3. Steenfelt, A. High-technology metals in alkaline and carbonatitic rocks in Greenland—recognition and exploration. *J. Geochem. Explor.* **1991**, *40*, 263–279. [CrossRef]
4. Ohnenstetter, D.; Piantone, P. Pyrochlore-Group Minerals in the Beauvoir Peraluminous Leukogranite, Massif-Central, France. *Can. Miner.* **1992**, *30*, 771–784. Available online: http://www.scopus.com/inward/record.url?eid=2-s2.0-0027047976&partnerID=MN8TOARS (accessed on 5 February 2022).
5. Aurisicchio, C.D.; De Vito, C. Nb and Ta oxide minerals in the Fonte del Prete granitic pegmatite dike, Island of Elba, Italy. *Can. Miner.* **2002**, *40*, 799–814. [CrossRef]
6. Cerny, P.; Chapman, R.; Ferreira, K.; Smeds, S.A. Geochemistry of oxide minerals of Nb, Ta, Sn, and Sb in the Varutrask granitic pegmatite, Sweden: The case of an "anomalous" columbite-tantalite trend. *Am. Miner.* **2004**, *89*, 505–518. [CrossRef]
7. Torro, L.; Villanova, C.; Castillo, M.; Campeny, M.; Goncalves, A.O.; Melgarejo, J.C. Niobium and rare earth minerals from the Virulundo carbonatite, Namibe, Angola. *Miner. Mag.* **2012**, *76*, 393–409. [CrossRef]
8. Salvi, S.; Williams, J.A.E. The role of hydrothermal processes in the granite hosted Zr, Y, REE deposit at Strange Lake, Quebec/Labrador: Evidence from fluid inclusions. *Geochim. Cosmochim. Acta* **1990**, *54*, 2403–2418. [CrossRef]
9. Salvi, S.; Williams, J.A.E. Alteration, HFSE mineralization and hydrocarbon formation in peralkaline igneous systems: Insights from the Strange Lake Pluton, Canada. *Lithos* **2006**, *91*, 19–34. [CrossRef]
10. Liu, Y.; Hou, Z. A synthesis of mineralization styles with an integrated genetic model of carbonatite-syenite-hosted REE deposits in the Cenozoic Mianning-Dechang REE metallogenic belt, the eastern Tibetan Plateau, southwestern China. *J. Asian Earth Sci.* **2017**, *137*, 35–79. [CrossRef]
11. Kirwin, D. Granite-related ore deposits. *Econ. Geol.* **2012**, *107*, 383–384. [CrossRef]
12. Dostal, J.; Shellnutt, J.G. Origin of peralkaline granites of the Jurassic Bokan Mountain complex (southeastern Alaska) hosting rare metal mineralization. *Int. Geol. Rev.* **2015**, *58*, 1–13. [CrossRef]
13. Salvi, S.; Williams, J.A.E. The role of hydrothermal processes in concentrating high-field strength elements in the Strange Lake peralkaline complex, northeastern Canada. *Geochim. Cosmochim. Acta* **1996**, *60*, 1917–1932. [CrossRef]
14. Schmitt, A.K.; Trumbull, R.B.; Dulski, P.; Emmermann, R. Zr-Nb-REE Mineralization in Peralkaline Granites from the Amis Complex, Brandberg (Namibia): Evidence for Magmatic Pre-enrichment from Melt Inclusions. *Econ. Geol.* **2002**, *97*, 399–413. [CrossRef]
15. Williams, J.A.E.; Migdisov, A.A.; Samson, I.M. Hydrothermal mobilisation of the Rare Earth Elements—A Tale of "Ceria" and "Yttria". *Elements* **2012**, *8*, 355–360. [CrossRef]
16. Dostal, J.; Kontak, D.J.; Karl, S.M. The early Jurassic Bokan Mountain peralkaline granitic complex (southeastern Alaska): Geochemistry, petrogenesis and rare-metal mineralization. *Lithos* **2014**, *202–203*, 395–412. [CrossRef]
17. Sun, Z.H.; Qin, K.Z.; Mao, Y.J.; Tang, D.M.; Ma, D.C. Characteristics and significance of aegirine and arfvedsonite in Boziguoer Nb-Ta-Zr-Rb-REE deposit related to alkaline granite, Xinjiang. *Acta Petrol. Sin.* **2021**, *37*, 3687–3711. (In Chinese with English Abstract)
18. Xu, H.M.; Fang, J.L.; Wang, J.; Fan, L. Geological characteristics of Boziguoer Niobium-tantalum deposit in Xinjiang. *Miner. Depos.* **2010**, *29*, 309–310. (In Chinese)

19. Xu, H.M.; Zou, T.R.; Fang, J.L.; Xu, J.; Fan, L.; Wang, J. Age and genesis of Boziguoer Niobium-tantalite deposit in Xinjiang. *Miner. Depos.* **2012**, *31*, 625–626. (In Chinese)
20. Yin, J.W.; Li, G.W.; Yang, G.M.; Ge, X.K.; Xu, H.M.; Wang, J. Fluornatropyrochlore, a new pyrochlore supergroup mineral from the Boziguoer rare earth element deposit, Baicheng county, Akesu, Xinjiang, China. *Can. Miner.* **2015**, *53*, 455–460. [CrossRef]
21. Ogunleye, P.O.; Garba, I.; Ike, E.C. Factors contributing to enrichment and crystallization of niobium in pyrochlore in the Kaffo albite arfvedsonite granite, Ririwai Complex, Younger Granites province of Nigeria. *J. Afr. Earth Sci.* **2006**, *44*, 372–382. [CrossRef]
22. Krishnamurthy, P.; Hoda, S.Q.; Sinha, R.P.; Banerjee, D.C.; Dwivedy, K.K. Economic aspects of carbonatites of India. *J. Asian Earth Sci.* **2000**, *18*, 229–235. [CrossRef]
23. Cordeiro, P.F.O.; Brod, J.A.; Palmieri, M.; Oliveira, C.G.; Barbosa, E.S.R.; Santo, R.V. The Catalão I niobium deposit, central brazil: Resources, geology and pyrochlore chemistry. *Ore Geol. Rev.* **2011**, *41*, 112–121. [CrossRef]
24. Mackay, D.A.R.; Simandl, G.J. Pyrochlore and columbite-tantalite as indicator minerals for specialty metal deposits. *Geochem. Explor. Environ. Anal.* **2015**, *15*, 167–178. [CrossRef]
25. Mitchell, R.H. Primary and secondary niobium mineral deposits associated with carbonatites. *Ore Geol. Rev.* **2015**, *64*, 626–641. [CrossRef]
26. Liu, C.H.; Yin, J.W.; Wu, C.L.; Cai, J.; Shao, X.K.; Yang, H.T.; Gao, Y.H.; Lei, M.; Xu, H.M.; Wang, J. Mineralogy and temperature of magma generation for A-type granitoids in Boziguoer, Baicheng County, Xinjiang. *Acta Petrol. Sin.* **2012**, *31*, 589–602. (In Chinese with English Abstract)
27. Liu, C.H.; Wu, C.L.; Gao, Y.H.; Lei, M.; Qin, H.P.; Li, M.Z. Zircon LA-ICP-MS U-Pb dating and Lu-Hf isotopic system of A-type granitoids in South Tianshan, Baicheng County, Xinjiang. *Acta Petrol. Sin.* **2014**, *30*, 1595–1614. (In Chinese with English Abstract)
28. Yin, J.; Shao, X.; Yang, H.; Piao, T.; Xu, H.; Wang, J. Radioactive mineral characteristics of Boziguoer alkaline rocks in Baicheng, Xinjiang. *Miner. Depos.* **2013**, *32*, 337–352. (In Chinese with English Abstract) [CrossRef]
29. Yin, J.; Yan, X.; Park, J.; Hou, F.; Chen, P.; Nie, X.; Xu, H.; Wang, J. Mineralogical characteristics of intrusive rocks in Boziguoer east mining area, Baicheng county, Xinjiang. *Earth Sci. J. China Univ. Geosci.* **2014**, *39*, 251–260. (In Chinese with English Abstract)
30. Hogarth, D.D.; Horne, J.E.T. Non-metamict uranoan pyrochlore and uranpyrochlore from tuff near Ndale, Fort Portal area, Uganda. *Miner. Mag.* **1989**, *53*, 257–262. [CrossRef]
31. Lumpkin, G.R.; Ewing, R.C. Geochemical alteration of pyrochlore group minerals. pyrochlore subgroup. *Am. Miner.* **1995**, *80*, 732–743. [CrossRef]
32. Williams, C.T.; Wall, F.; Woolley, A.R.; Phillipo, S. Compositional variation in pyrochlore from the Bingo carbonatite, Zaire. *J. Afr. Earth Sci.* **1997**, *25*, 137–145. [CrossRef]
33. Hogarth, D.D.; Williams, C.T.; Jones, P. Primary zoning in pyrochlore group minerals from carbonatites. *Miner. Mag.* **2000**, *64*, 683–697. [CrossRef]
34. Nasraoui, M.; Bilal, E. Pyrochlore from the Lueshe carbonatite complex (Democratic Republic of Congo): A geochemical record of different alteration stages. *J. Asian Earth Sci.* **2000**, *18*, 237–251. [CrossRef]
35. Chakhmouradian, A.R.; Mitchell, R.H. New data on pyrochlore- and perovskite-group minerals from the Lovozero alkaline complex, Russia. *Eur. J. Miner.* **2002**, *14*, 821–836. [CrossRef]
36. Zurevinski, S.E.; Mitchell, R.H. Extreme compositional variation of pyrochlore group minerals at the Oka carbonatite complex, Quebec: Evidence of magma mixing. *Can. Miner.* **2004**, *42*, 1159–1168. [CrossRef]
37. Lee, M.J.; Lee, J.I.; Garcia, D.; Moutte, J.; Williams, C.T.; Wall, F.; Kim, Y. Pyrochlore chemistry from the Sokliphoscorite–carbonatite complex, Finland: Implications for the genesis of phoscorite and carbonatite association. *Geochem. J.* **2006**, *40*, 1–13. [CrossRef]
38. Bambi, A.C.J.M.; Costanzo, A.; Goncalves, A.O.; Melgarejo, J.C. Tracing the chemical evolution of primary pyrochlore from plutonic to volcanic carbonatites: The role of fluorine. *Miner. Mag.* **2012**, *76*, 377–392. [CrossRef]
39. Zaitsev, A.N.; Williams, C.T.; Wall, F.; Zolotarev, A.A. Evolution of chemical composition of pyrochlore group minerals from phoscorites and carbonatites of the khibina alkaline massif. *Geol. Ore Deposit.* **2012**, *54*, 503–515. [CrossRef]
40. McCreath, J.A.; Finch, A.A.; Herd, D.A.; Armour, B.A. Geochemistry of pyrochlore minerals from the Motzfeldt Center, South Greenland: The mineralogy of a syenite-hosted Ta Nb deposit. *Am. Miner.* **2013**, *98*, 426–438. [CrossRef]
41. Walter, B.F.; Parsapoor, A.; Braunger, S.; Marks, M.A.W.; Wenzel, T.; Martin, M.; Markl, G. Pyrochlore as a monitor for magmatic and hydrothermal processes in carbonatites from the Kaiserstuhl volcanic complex (SW Germany). *Chem. Geol.* **2018**, *498*, 1–16. [CrossRef]
42. Jahn, B.M.; Griffin, W.L.; Windley, B. Continental growth in the Phanerozoic: Evidence from Central Asia. *Tectonophysics* **2000**, *328*, 5–7. [CrossRef]
43. Han, B.F.; Ji, J.Q.; Song, B.; Chen, L.H.; Zhang, L. Late Paleozoic vertical growth of continental crust around the Junggar Basin, Xinjiang, China (Part I): Timing of post- collisional plutonism. *Acta Petrol. Sin.* **2006**, *22*, 1077–1086. (In Chinese with English abstract)
44. Qin, K.Z.; Su, B.X.; Patrick, A.S.; Tang, D.M.; Li, X.H.; Sun, H.; Xiao, Q.H.; Liu, P.P. SIMS zircon U-Pb geochronology and Sr-Nd isotopes of Ni-Cu-bearing mafic-ultramafic intrusions in Eastern Tianshan and Beishan in correlation with flood basalts in Tarim Basin (NW China): Constraints on a ca. 280 Ma mantle plume. *Am. J. Sci.* **2011**, *311*, 237–260. [CrossRef]
45. Qin, K.Z.; Tang, D.M.; Su, B.X.; Mao, Y.J.; Xue, S.C.; Tian, Y.; Sun, H.; San, J.Z.; Xiao, Q.H.; Deng, G. The tectonic setting, style, basic feature, relative erosion degree, ore-bearing evaluation sign, potential analysis of mineralization of Cu-Ni-bearing Permian mafic-ultramafic complexes, Northern Xinjiang. *Northwest. Geol.* **2012**, *45*, 83–116. (In Chinese with English Abstract)

46. Qin, K.Z.; Zhai, M.G.; Li, G.M.; Zhao, J.X.; Zeng, Q.D.; Gao, J.; Xiao, W.J.; Li, J.L.; Sun, S. Links of Collage orogenesis of multiblocks and crust evolution to characteristic metallogeneses in China. *Acta Petrol. Sin.* **2017**, *33*, 305–325. (In Chinese with English Abstract)
47. Su, B.X.; Qin, K.Z.; Patrick, A.S.; Li, X.H.; Yang, Y.H.; Sun, H.; Tang, D.M.; Liu, P.P.; Xiao, Q.H.; Malaviarachchi, S.P.K. U-Pb ages and Hf-O isotopes of zircons from Late Paleozoic mafic-ultramafic units in the southern Central Asian Orogenic Belt: Tectonic implications and evidence for an Early-Permian mantle plume. *Gondwana Res.* **2011**, *20*, 516–531. [CrossRef]
48. Su, B.X.; Qin, K.Z.; Sakyi, P.A.; Liu, P.P.; Tang, D.M.; Malaviarachchi, S.P.K.; Xiao, Q.H.; Sun, H.; Dai, Y.C.; Hu, Y. Geochemistry and geochronology of acidic rocks in the Beishan region, NW China: Petrogenesis and tectonic implications. *J. Asian Earth Sci.* **2011**, *41*, 31–43. [CrossRef]
49. Qin, K.Z.; Sun, S.; Li, J.L.; Fang, T.H.; Wang, S.L.; Liu, W. Paleozoic epithermal Au and porphyry Cu Deposits in North Xinjiang, China: Epochs, Features, Tectonic Linkage and Exploration Significance. *Resour. Geol.* **2002**, *52*, 291–300. [CrossRef]
50. Li, J.Y.; He, G.Q.; Xu, X.; Li, H.Q.; Sun, G.H.; Yang, T.N.; Gao, L.M.; Zhu, Z.X. Crustal Tectonic Framework of Northern Xinjiang and Adjacent Regions and Its Formation. *Acta Geol. Sin. Engl.* **2006**, *80*, 148–168. (In Chinese with English Abstract)
51. Yang, T.N.; Li, J.Y.; Sun, G.H.; Wang, Y.B. Earlier Devonian active continental arc in Central Tianshan: Evidence of geochemical analyses and Zircon SHRIMP dating on mylonitized granitic rock. *Acta Petrol. Sin.* **2006**, *22*, 41–48. (In Chinese with English Abstract)
52. Zhu, Z.X.; Wang, K.Z.; Xu, D.; Su, Y.L.; Wu, Y.M. SHRIMP U-Pb dating of zircons from Carboniferous intrusive rocks on the active continental margin of Eren Habirga, West Tianshan, Xinjiang, China, and its geological implications. *Geol. Bull. China* **2006**, *25*, 986–991. (In Chinese with English Abstract)
53. Xiao, W.J.; Han, C.M.; Yuan, C. Middle Cambrian to Permian subduction-related accretionary orogenesis of northern Xinjiang, NW China: Implications for the tectonic evolution of Central Asia. *J. Asian Earth Sci.* **2008**, *32*, 102–117. [CrossRef]
54. Xiao, W.J.; Huang, B.C.; Han, C.M. A review of the western part of the Altaids: A key to understanding the architecture of accretionary orogens. *Gondwana Res.* **2010**, *18*, 253–273. [CrossRef]
55. Zhang, C.L.; Li, Z.X.; Li, X.H.; Ye, H.M. Neoproterozoic mafic dyke swarms at the northern margin of the Tarim Block, NW China: Age, geochemistry, petrogenesis and tectonic implications. *J. Asian Earth Sci.* **2009**, *35*, 167–179. [CrossRef]
56. Tong, Y.; Wang, T.; Hong, D.W.; Han, B.F.; Zhang, J.J.; Shi, X.J.; Wang, C. Spatial and temporal distribution of the Carboniferous-Permian granitoids in northern Xinjiang and its adjacent areas, and its tectonic significance. *Acta Petrol. Et Mineral.* **2010**, *29*, 619–641. (In Chinese with English Abstract)
57. Huang, H.; Zhang, Z.C.; Zhang, D.Y.; Du, H.X.; Ma, L.T.; Kang, J.L.; Xue, C.J. Petrogenesis of Late Carboniferous to Early Permian Granitoid Plutons in the Chinese South Tianshan: Implications for Crustal Accretion. *Acta Geol. Sin.* **2011**, *85*, 1305–1333. (In Chinese with English Abstract)
58. Zong, Z.J.; Du, Y.S.; Li, S.T.; Cao, Y.; Du, J.G.; Deng, X.H.; Xue, L.W. Petrogenesis of the early Permian A-type granites in the Halajun region, southwest Tianshan, western Xinjiang, NW China: Implications for geodynamics of Tarim large igneous province. *Int. Geol. Rev.* **2020**, *63*, 1110–1131. [CrossRef]
59. Gao, J.; Long, L.L.; Qian, Q.; Huang, D.Z.; Su, W.; Klemd, R. South Tianshan: A Late Paleozoic or a Triassic orogen. *Acta Petrol. Sin.* **2006**, *22*, 1049–1061. (In Chinese with English Abstract)
60. Liu, C.X.; Xu, B.L.; Zou, T.R.; Lu, F.X.; Tong, Y.; Cai, J.H. Petrochemistry and tectonic significance of Hercynian alkaline rocks along the northern margin of the Tarim platform and its adjacent area. *Xinjiang Geol.* **2004**, *22*, 43–49. (In Chinese with English Abstract)
61. Zou, T.R.; Li, Q.C. *Rare and Rare Earth Metallic Deposits in Xinjiang, China*; Geological Publishing House: Xinjiang, China, 2006. (In Chinese)
62. Zou, T.R.; Xu, J.; Chen, W.S.; Xia, F.R. Rare and rare earth mineral deposits related to alkaline rocks on northern margin of Tarim Basin, Xinjing, China. *Miner. Depos.* **2002**, *21*, 845–848. (In Chinese with English Abstract)
63. Huang, H.; Zhang, Z.C.; Santosh, M.; Zhang, D.Y. Geochronology, geochemistry and metallogenic implications of the Boziguo'er rare metal-bearing peralkaline granitic intrusion in South Tianshan, NW China. *Ore Geol. Rev.* **2014**, *61*, 157–174. [CrossRef]
64. Droop, G.T.R. A general equation for estimating Fe^{3+} concentrations inferromagnesian silicates and oxides from microprobe analyses, using stoichiometric criteria. *Miner. Mag.* **1987**, *51*, 431–436. [CrossRef]
65. Liu, X.M.; Gao, S.; Diwu, C.R.; Ling, W.L. Precambrian crustal growth of Yangtze craton as revealed by detrital zircon studies. *Am. J. Sci.* **2008**, *308*, 421–468. [CrossRef]
66. Atencio, D.; Andrade, M.B.; Christy, A.G.; Gieré, R.; Kartashov, P.M. The pyrochlore supergroup of minerals: Nomenclature. *Can. Miner.* **2010**, *48*, 673–698. [CrossRef]
67. Caprilli, E.; Della Ventura, G.; Williams, T.C.; Parodi, G.C.; Tuccimei, P. The crystal chemistry of non-metamict pyrochlore-group minerals from Latium, Italy. *Can. Miner.* **2006**, *44*, 1367–1378. [CrossRef]
68. Wall, F.; Williams, C.T.; Woolley, A.R.; Nasraoui, M. Pyrochlore from weathered carbonatite at Lueshe, Zaire. *Miner. Mag.* **1996**, *60*, 731–750. [CrossRef]
69. Hogarth, D.D. Classification and nomenclature of the pyrochlore group. *Am. Miner.* **1977**, *62*, 403–410.
70. Finch, A.A.; McCreath, J.A.; Reekie, C.D.J.; Hutchison, W.; Ismaila, A.; Armour, B.A.; Andersen, T.; Simonsen, S.L. From mantle to Motzfeldt: A genetic model for syenite-hosted Ta Nb-mineralisation. *Ore Geol. Rev.* **2019**, *107*, 402–416. [CrossRef]
71. Sun, S.S.; McDonough, W.F. Chemical and isotopic systematics of oceanic basalts: Implications for mantle composition and processes. *Geol. Soc. Lond. Spec. Publ.* **1989**, *42*, 313–345. [CrossRef]
72. Chakhmouradian, A.R.; Mitchell, R.H. Lueshite, pyrochlore and monazite-(Ce) from apatite–dolomite carbonatite, LesnayaVaraka complex, Kola Peninsula, Russia. *Miner. Mag.* **1998**, *62*, 769–782. [CrossRef]

73. Chakhmouradian, A.R.; Williams, C.T. Mineralogy of high-field-strength elements (Ti, Nb, Zr, Ta, Hf) in phoscoritic and carbonatitic rocks of the Kola Peninsula, Russia. I. In *Phoscorites and Carbonatites from Mantle to Mine: The Key Example of the Kola Alkaline Province*; Wall, F., Zaitsev, A.N., Eds.; Mineralogical Society Series: London, UK, 2004; pp. 293–340.
74. Chakhmouradian, A.R. High-field-strength elements in carbonatitic rocks: Geochemistry, crystal chemistry and significance for constraining the sources of carbonatites. *Chem. Geol.* **2006**, *235*, 138–160. [CrossRef]
75. Chakhmouradian, A.R.; Reguir, E.P.; Kressall, R.D.; Crozier, J.; Pisiak, L.K.; Sidhu, R.; Yang, P. Carbonatite-hosted niobium deposit at Aley, northern British Columbia (Canada): Mineralogy, geochemistry and petrogenesis. *Ore Geol. Rev.* **2015**, *64*, 642–666. [CrossRef]
76. Lumpkin, G.R.; Ewing, R.C.; Williams, C.T.; Mariano, A.N. An overview of the crystal chemistry, durability, and radiation damage effects of natural pyrochlore. *MRS Proc.* **2000**, *663*, 921. [CrossRef]
77. Khromova, E.A.; Doroshkevich, A.G.; Sharygin, V.V.; Izbrodin, L.A. Compositional Evolution of Pyrochlore-Group Minerals in Carbonatites of the Belaya Zima Pluton, Eastern Sayan. *Geol. Ore Deposit.* **2017**, *59*, 752–764. [CrossRef]
78. Yaroshevskii, A.A.; Bagdasarov, Y.A. Geochemical diversity of minerals of the pyrochlore group. *Geochem. Int.* **2008**, *12*, 1322–1345. [CrossRef]
79. Stephan, K.; Jasper, B. Trace element partitioning between pyrochlore, microlite, fersmite and silicate melts. *Geochem. Trans.* **2020**, *21*, 9. [CrossRef]
80. Anenburg, M.; Williams, M.J. Quantifying the Tetrad Effect, Shape Components, and Ce–Eu–Gd Anomalies in Rare Earth Element Patterns. *Math. Geosci.* **2022**, *54*, 47–70. [CrossRef]
81. Knudsen, C. Pyrochlore group minerals from the Qaqarssuk carbonatite complex. Lanthanides. In *Tantalum and Niobium*; Möller, P., Cerný, P., Saupé, F., Eds.; Springer: Berlin/Heidelberg, Germany, 1989; pp. 80–99. [CrossRef]
82. Anderson, T. Evolution of peralkaline calcite carbonatite magma in the Fen Complex, Southeast Norway. *Lithos* **1988**, *22*, 99–112. [CrossRef]
83. Wolfe, J.A. Crystallization of nepheline syenite in a subvolcanic magma system: Tenerife, Canary Islands. *Lithos* **1987**, *20*, 207–223. [CrossRef]
84. Woolley, A.R.; Platt, R.G. The mineralogy of nepheline syenite complexes from the northern part of the Chilwa province Malawi. *Miner. Mag.* **1986**, *50*, 597–610. [CrossRef]